Vapor liquid equilibrium of pure and aqueous Methyl diethanolamine (MDEA), 2-Dimethylmonoethanolamine (DMMEA), N-Methylmonoethanolamine (MMEA) and 1-(2-Aminoethyl)piperazine (AEP) : Experimental results and modeling.

Hallvard F. Svendsen[1], Øystein Jonassen[1], Ardi Hartono[1], Usman Shoukat[1], Maxime Francois[1], Hanna K. Knuutila[1] and Inna Kim[2]*

[1]Norwegian University of Science and Technology, Sem Sælands vei 4, NO7491 Trondheim, Norway

[2]SINTEF Industry, P.O. Box 4760 Torgarden, NO-7465 Trondheim, Norway

Abstract

This work presents new vapor-liquid data for the pure components 2-dimethylmonoethanolamine (DMMEA) and N-methylethanolamine (MMEA) and for the binary systems of aqueous methyldiethanolamine (MDEA), DMMEA, MMEA, and 1-(2-aminoethyl)piperazine (AEP). New Antoine models are developed for the pure component systems, and new and improved NRTL models for the binary systems. In the model development, together with new data from this work, all available data on VLE, excess heat of mixing, H^E, freezing point depression, and specific heat were gathered, evaluated and used selectively for parameter optimization. Emphasis has been put on a best possible representation of amine volatility to enable reasonable predictions of amine emissions from absorption plants and to form a basis for subsequent models of ternary systems with CO_2. Model predictions are compared with experimental results and other models, source by source, and the overall results are satisfactory.

Keywords: Vapor-liquid equilibria; pure compounds; binary mixtures; MDEA; DMMEA, MMEA; AEP

1. Introduction

In spite of the ongoing search for improved chemicals for low-pressure CO_2 capture, there is still a need for new systems that, both energetically and environmentally, are better than the industrial standard, MEA (monoethanolamine). One of the promising developments has been a combination of a tertiary or hindered amine and a primary amine [1-3], exploiting the combination of low heat of reaction of the tertiary amine and the rapid kinetics of the primary amine.

Aqueous solutions based on the tertiary amine MDEA have been used for decades for CO_2 removal from intermediate and high-pressure gas streams, both alone and together with kinetic promotors, e.g. the BASF aMDEA solutions, see Appl et al. (1982) [4]. However, MDEA is classified as a "red" chemical according to the Convention for the Protection of the Marine Environment of the North-East Atlantic (OSPAR Convention). The Norwegian Activities Regulation (PSA, 2010) states minimum recommended values of 20% biodegradability, an EC50/LC50 value of ≥10 mg/l in acute ecotoxicity, and a bioaccumulation potential of log Pow < 3. Haugmo et al. (2009 and 2012) [5, 6], show that the acute ecotoxicity level of MDEA is within the given limit but the biodegradability is so low that the chemical should be phased out. Search for an alternative chemical has been ongoing, and DMMEA has been found to have both low ecotoxicity and satisfactory biodegradability, see Haugmo et al. (2009 and 2012) [5, 6]. Also, Henni et al. (2008) [7] found that DMMEA is a faster reactant than MDEA and Hedayati and Feyzi (2021) [8] found it to be an interesting chemical in mixtures.

Both alone and as a promoter, piperazine has been suggested for low pressure CO_2 capture, see Rochelle et al. (2011) [9] , but its secondary nature renders it susceptible to forming nitrosamines. MMEA, (Ernst et al. (1971) [10], and AEP, (Du and Rochelle (2014) [11], Dey et al. (2019) [12]), have been suggested as promoters. MMEA has low ecotoxicity and high

biodegradability according to Haugmo et al. (2009, 2012) [5, 6, 9], whereas AEP was not tested in this respect. AEP is also the main degradation product of Piperazine, see Freeman et al. (2010) [13] and Mazari et al. (2014) [14].

This paper presents new pure component and binary VLE data for the DMMEA-water and the MMEA-water systems, and binary data for MDEA-water and AEP-water, based on ebulliometric measurements. The new binary data for MDEA span a range in temperature from 313 to 373K and MDEA mole fractions from 0.05 to about 0.8, for DMMEA: 333 to 373K in temperature and 0.02 to 0.22 in mole fraction, for MMEA: 313 to 373K in temperature and 0.01 to 0.34 in mole fraction and for AEP: 313 to 373K in temperature and 0.001 to 0.23 in mole fraction.

Based on data from this work and a thorough review of existing pure component and binary data, new Antoine and NRTL parameters were fitted for the pure components and binary systems respectively. In the binary parameter regression, emphasis was put on improved representation of amine volatility to further on improve the accuracy of ternary models with CO_2 and emissions predictions.

2. Experimental methods

2.1. Materials, procedures and uncertainties

The chemicals used were purchased from Sigma Aldrich, with purities as given in Table 1 and used as received in this work. Water analyses on the received amines were performed by Karl Fisher titration and results are shown in table 1. Two parallel samples were analyzed, and the differences varied from 1 to 2% for the high concentrations to up to 9% for the lowest water content. For AEP the water content is higher than expected from the Certificate of Analysis (COA). This may be caused by uncertainty in the water analysis or in the COA.

Table 1. Chemicals used

Abbreviation	Name	CAS number	Purity*, mass%	Water content, mass%
MDEA	Methyldiethanolamine	105-59-9	>99.9	0.081
DMMEA	2-Dimethylmonoethanolamine	108-01-0	>99.9	0.046
MMEA	N-Methylethanolamine	109-83-1	>99.7	0.221
AEP	1-(2-Aminoethyl) piperazine	140-31-8	>99.8	0.337

*Taken from the COA (Certificate of Analysis) delivered by the supplier.

Aqueous solutions were prepared gravimetrically by mixing with distilled and deionized water with resistivity 18.2 $M\Omega \cdot cm$. The experiments in this work cover the composition ranges: 0.03 to 97 mass % for MDEA, 0.085 to 49 mass % for DMMEA, 0.09 to 49 mass % for MMEA and 0.1 to 84 mass % for AEP, and the temperature span 40 to100ºC. This work, together with data from the literature covers almost the whole concentration range for all four components.

For both pure component and binary mixture measurements, a modified Swietoslawski ebulliometer, as described by Rogalski and Malanowski (1980) [15], was used. The procedure used is the same as described in detail in Kim et al. (2008) [16] and later in Hartono et al. [17-20], and is not elaborated in this work. It should only be noted that the ebulliometer was charged with amine, brought to boiling while evacuated, and then cooled and emptied several times, until a stable pressure reading was obtained. In this way, the pressure contribution from remaining water in the apparatus is avoided and water in the original amine mostly removed. This is most effective and most important for the least volatile amines. The temperature measurements were performed using a Pt-100 temperature sensor with accuracy ±0.05K and the pressures were measured using a DPI520 (Druck, Germany) pressure sensor with accuracy ±0.15 kPa.

The liquid phase samples were analyzed by titration with aqueous 0.1(~0.976 mass %) or 0.01(~0.098 mass %) mol/dm^3 H_2SO_4 using a standard procedure with a Titrando 809 (Metrohm AG, Switzerland) potentiometric titrator. Two samples were always titrated and if the difference was more that 3% a third sample was titrated. The lower limit for this procedure was a mole fraction of about 0.0002. This was sufficient for all liquid phase analyses. Vapor samples, condensate, were also titrated with the same procedure for concentrations above 0.0004 in mole fraction. For lower concentrations, they were analyzed using LCMS-MS with accuracy of ±5% and with a detection limit of about 10^{-8} in mole fraction, (0.5 μmole/L).

In addition to the T, P and analytical uncertainties, the gas phase condensate sampling could introduce uncertainties much larger than the actual analyses, particularly for the low-volatility components. This is further discussed under the individual components result sections. The estimated standard uncertainties are given in the result tables.

2.2. Thermodynamic model

In this work, the pure component saturation pressures were modelled using an Antoine equation [21] :

$$P_i^{sat}/\mathrm{Pa} = 10^{(A-\frac{B}{C+T})} \quad (1)$$

Where P_i^{sat} is the component saturated vapor pressure in Pa, T is the temperature in K and A, B and C are fitted parameters.

The binary aqueous amine equilibria were modelled using the NRTL model based on the excess Gibbs energy, see Renon and Prausnitz (1968) [22], Prausnitz et al., (1999) [23] and Schmidt et al (2007) [24]:

$$G^E = x_1 \cdot x_2 \cdot \left(\frac{\tau_{21} \cdot G_{21}}{x_1 + x_2 \cdot G_{21}} + \frac{\tau_{12} \cdot G_{12}}{x_2 + x_1 \cdot G_{21}}\right) \quad (2)$$

where:

$$\tau_{12} = a_{12} + \frac{b_{12}}{T}, \quad \tau_{21} = a_{21} + \frac{b_{21}}{T} \tag{3}$$

and

$$G_{12} = exp(-\alpha_{12} \cdot \tau_{12}), \quad G_{21} = exp(-\alpha_{21} \cdot \tau_{21}) \tag{4}$$

Here a_{12}, a_{21}, b_{12} and b_{21} are energy parameters describing the interaction between components i and j, and $\alpha_{ij} = \alpha_{ji}$ are the non-randomness parameters.

The activity coefficients are then given as:

$$ln\,\gamma_1 = x_2^2 \cdot \left[\tau_{21} \cdot \left(\frac{G_{21}}{x_1 + x_2 \cdot G_{21}}\right)^2 + \left(\frac{\tau_{12} \cdot G_{12}}{(x_2 + x_1 \cdot G_{12})^2}\right)\right] \tag{5}$$

$$ln\,\gamma_2 = x_1^2 \cdot \left[\tau_{12} \cdot \left(\frac{G_{12}}{x_2 + x_1 \cdot G_{12}}\right)^2 + \left(\frac{\tau_{21} \cdot G_{21}}{(x_1 + x_2 \cdot G_{21})^2}\right)\right] \tag{6}$$

The equation for excess heat of mixing then becomes:

$$\mathrm{H}^E = -R\left(\frac{x_1 \cdot x_2 \cdot b_{21} \cdot G_{21} \cdot (x_1 \cdot (\alpha_{12} \cdot \tau_{21} - 1) - x_2 \cdot G_{21})}{(x_1 + x_2 \cdot G_{21})^2} + \frac{x_1 \cdot x_2 \cdot b_{12} \cdot G_{12} \cdot (x_2 \cdot (\alpha_{12} \cdot \tau_{12} - 1) - x_1 \cdot G_{12})}{(x_2 + x_1 \cdot G_{12})^2}\right) \tag{7}$$

The phase equilibrium is solved using a so-called $\gamma - \phi$ approach. This means that the non-idealities are corrected by introducing activity coefficients for the liquid phase and fugacity coefficients for the gas phase. The thermodynamic expression used for calculating the vapor-liquid equilibrium is:

$$P \cdot y_i \cdot \phi_i^V = x_i \cdot \gamma_i \cdot P_i^{sat} \cdot \phi_i^{sat} \cdot exp\left(\int_{P_i^{vap}}^{P} \frac{V_i^L \cdot dp}{R \cdot T}\right) \tag{8}$$

In equation (8) the Raoult's law reference state is used. The exponential term in equation (8) is the so-called Pointing correction factor, which corrects a liquid being at a pressure other than its saturation pressure. At low pressures, this factor is close to one, but at higher pressures, it can have a significant effect. In this work, it was set to 1. Also, the liquid fugacity coefficient, ϕ_i^{sat} is assumed 1. The activity coefficients are calculated using the NRTL model just

described, while the Peng-Robinson (1976) [25] equation of state is used to calculate the fugacity coefficients. The binary interaction parameters in the Peng-Robinson equation were set to zero.

The objective function used to regress the NRTL parameters was the absolute average relative deviation function on the variables used for the regression, see Schmidt et al. (2007) [24]:

$$AARD = \frac{W_P}{N_P}\sum_{i=1}^{N_P}\frac{\left|P_i^{calc}-P_i^{exp}\right|}{P_i^{exp}} + \frac{W_{He}}{N_{He}}\sum_{i=1}^{N_{He}}\frac{\left|H_i^{E,calc}-H_i^{E,exp}\right|}{H_i^{E,exp}} + \frac{W_{FPD}}{N_{FPD}}\sum_{i=1}^{N_{FPD}}\frac{\left|FPD_i^{calc}-FPD_i^{exp}\right|}{FPD_i^{exp}} + \frac{W_y}{N_y}\sum_{i=1}^{N_y}\frac{\left|y_{i,Amine}^{calc}-y_{i,Amine}^{exp}\right|}{y_{i,Amine}^{exp}} \quad (9)$$

Where the $N's$ are the number of data points of each category used in the regression, P_i^{calc}, $H_i^{E,calc}$, FPD_i^{calc} and y_i^{calc} are the calculated value of the pertinent data in point i and P_i^{exp}, $H_i^{E,exp}$, FPD_i^{exp} and y_i^{exp} are the experimentally determined values. The absolute average relative deviation (AARD) was also calculated for the individual data series. The weighing factors, W, were set to 1 in this work.

To regress parameters to experimental data, the PSO algorithm by Kennedy and Eberhart (1995) [26] was used as described in detail in Monteiro et al. (2013) [27]. In the binary parameter fitting we also regressed the randomness parameters to the available binary data, however, maintaining $\alpha_{12} = \alpha_{21}$. This was found by Schmidt et al., (2007) [24] to be the best overall approach.

3. Results

3.1. Pure components

The results for the individual compounds are first discussed. At the end, in Table 6, the obtained Antoine parameters and AARD's for the fits are given.

3.1.1. MDEA

Several sets of saturation pressure data for MDEA exist in the literature. The data used in fitting the Antoine parameters are given in Table 2.

Table 2: Data used for the regression of Antoine parameters for pure MDEA.

Source	Data type	Data points
Knorr and Matthes (1898) [28]	Static cell	1
Kim et al. (2008) [16]	Ebulliometer	7
Noll et al. (1998) [29]	Static cell	26
Soames et al. (2018) [30]	Ebulliometer	3
VonNiederhausern et al.(2006) [31]	Flow method	9

The fit to the available data is shown in Figure 1.

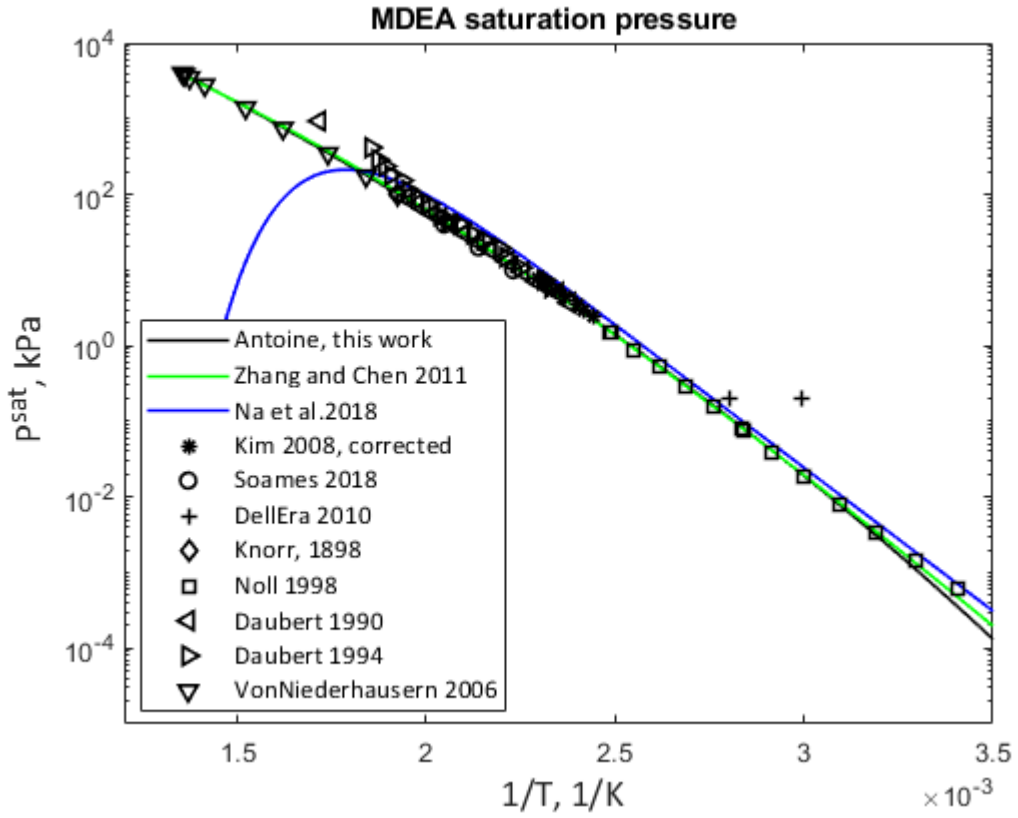

Figure 1. Model fit to available data for MDEA

Data from Dell'Era et al. (2010) [32], Daubert and Hutchison (1990) [33] and Daubert et al.(1994) are plotted in Figure 1 for comparison, but were not used in the fitting. The two data points from Dell'Era et al. (2010) [32] give the same saturation pressure for two temperatures about 25ºC apart. This could indicate that they may have reached a lower detection limit for their equipment. The points lie well above the regression curve in Figure 1. The two data sets from Daubert (1990 and 1994) [33, 34] are inconsistent and provide higher saturation pressures than the other sets. Daubert and Hutchison (1990) [33] noted that their MDEA decomposed above 250ºC. Thus, the data points above this temperature should be considered carefully. Also VonNiederhausern and Gmeling (2006) [35] excluded the data from Daubert (1990 and 1994) [33, 34] from their regression. Knorr and Matthes (1898) [28] provided one data point at 747 mmHg, giving the boiling point at 246 to 248ºC. The value 247ºC was used in Figure 2 and in

the fit. One problem with MDEA is its very low vapor pressure and the fact that most measurements have been performed with MDEA as received from the supplier. MDEA from the supplier will typically have purities above 99 mass % and part of the impurity will be water. Knorr and Matthes (1898) [28] observed that pure MDEA, exposed to ambient air for 1-3 hours, increased in weight. This strongly indicates that MDEA is hygroscopic. The hygroscopicity of amines is discussed in Touhara et al. (1982) [36]. The water content in MDEA used in our laboratory was measured by Skylogianni et al. (2020) [37] and in this work. Skylogianni et al. (2020) [37] found it to be below 0.2 mass% (1.3 mole %) and in this work it was determined to 0.081 mass% (0.5 mole %) as seen in Table 1. Apart from Noll et al. (1998) [29], none of the data sources listed in Table 2 purified the MDEA, but used it as received. Noll et al. (1998) [29] purified the MDEA by distillation under reduced pressure, and estimated the purity to be better than 99 mole%. Even low water contents, in the range of 0.1 to 0.2 mole %, may lead to errors, and the relatively significant deviations between the data sets for MDEA, compared to e.g. MMEA and DMMEA, may be ascribed to varying water content. In spite of this we have used the data sets chosen for regressing new Antoine parameters. The saturation pressure equations provided by Zhang and Chen (2011) [38] and Na et al. (2018) [39] are also shown in Figure 1. The curve for Zhang and Chen (2011) [38] gives saturation pressures very close to the Antoine equation from this work. The equation provided by Na et al. (2018) [39] gives about 20% higher saturation pressures at low temperatures, has a non-physical behavior at high temperatures, and should not be used.

As shown in Table 5, the AARD of the Antoine equation developed in this work is 4.1%, reflecting the uncertainty in the pure component pressure measurements.

3.1.2. DMMEA

For DMMEA, several sources of pure component vapor pressure data exist. The data are also more consistent with each other than was the case for MDEA. This is probably because of the higher volatility of DMMEA, and therefore obtaining data with good accuracy becomes easier. The data used for obtaining new Antoine parameters are given in Table 3

Table 3. Data used for regression of Antoine parameters for pure DMMEA.

Source	Data type	Data points
Touhara et al (1982) [36]	Static cell	2
Klepacova, et al. (2013) [40]	Ebulliometer	15
Chiali-Baba-Ahmed et al. (2013) [41]	Static cell	15
Quietzsch et al. (1970) [42]	Ebulliometer	3
This work	Ebulliometer	15

The model fit to experimental data is shown in Figure 2.

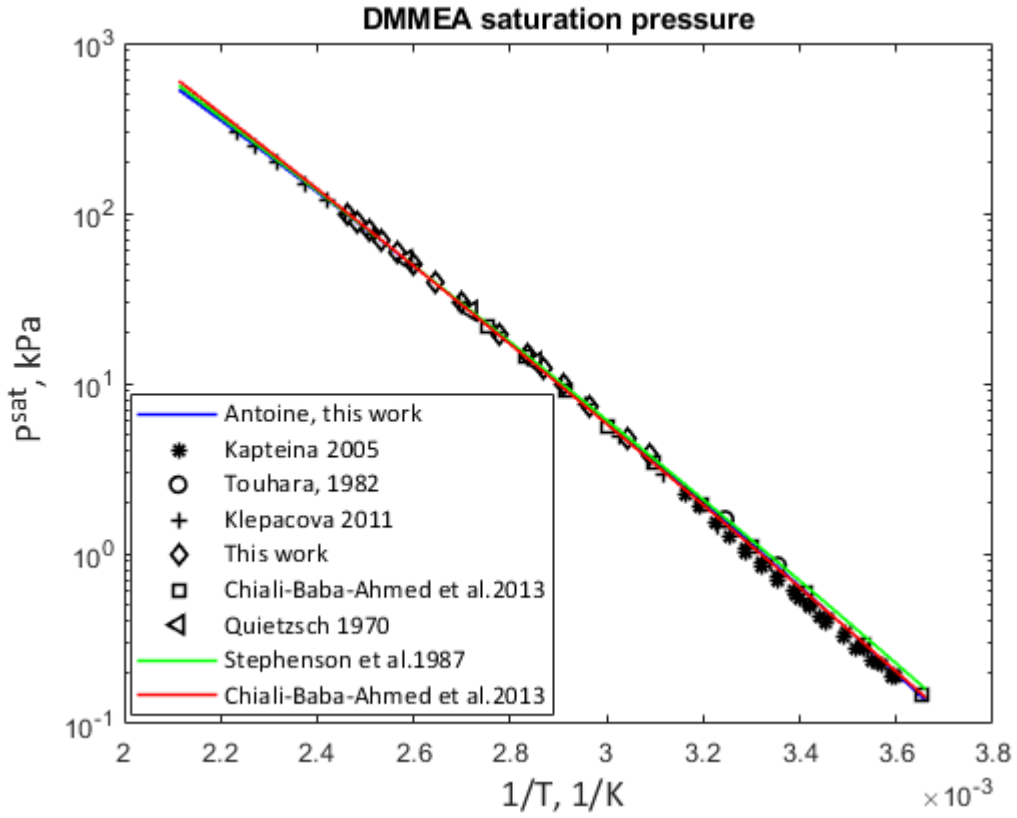

Figure 2. Model fit to available data for DMMEA

The data from Kapteina et al. (2005) [43] were not used in the parameter fitting but are plotted in Figure 2. From Figure 2, we see that almost all data points are very consistent, apart from the data from Kapteina et al. (2005) [43], which seem to be on the low side. This may be caused by the transpiration method used where it is difficult to ensure equilibrium in the exiting gas phase. A similar observation was made by Hartono et al. (2021) [44]. The DMMEA data from this work are given in Table A2 in the appendix both as measured and corrected values. The correction for the water content given in Table 1 was done by using the binary model to calculate the water pressure, which was subtracted from the measured total pressure to obtain the DMMEA pressure. The DMMEA saturation pressure was then calculated by dividing by mole fraction and activity coefficient. Bringas et al. (2015) [45] performed molecular dynamic simulations of DMMEA and calculated vapor pressures in good agreement with the experimental results shown in Figure 2.

The AARD for the fitted data was 1.8%. This is significantly lower than for MDEA, also indicating the consistency of the data. The data from Kapteina et al. (2005) [43] gave an AARD of 13%. The Antoine parameters given by Stephenson and Malanowski (1987) [46] fit well our new curve for high and intermediate temperatures, whereas at low temperatures, it seems to slightly over-predict the vapor pressures. The model by Chiali-Baba-Ahmed et al. (2013) (39) over-predicts the vapor pressures in the high-temperature range and under-predicts in the low-temperature range.

3.1.3. MMEA

Also, for MMEA, several sets of pure component saturation pressure data exist. Table 4 gives the sources of data used in the Antoine Parameter regression in this work. In addition, Riedel

equation parameters were taken from the DIPPR [47] database. The fit between the model and data is shown in Figure 3.

Table 4. Data used for regression of Antoine parameters for pure MMEA.

Source	Data type	Data points
Klepacova et al. (2011) [40]	Ebulliometer	16
Noll et al. (1998) [29]	Static cell	15
Touhara et al. (1982) [36]	Static cell	2
Steele et al. (1997) [48]	Ebulliometer	20
This work	Ebulliometer	10
Schotte et al. (1928) [49]	Static cell	1
Knorr and Matthes (1898) [28]	Static cell	1

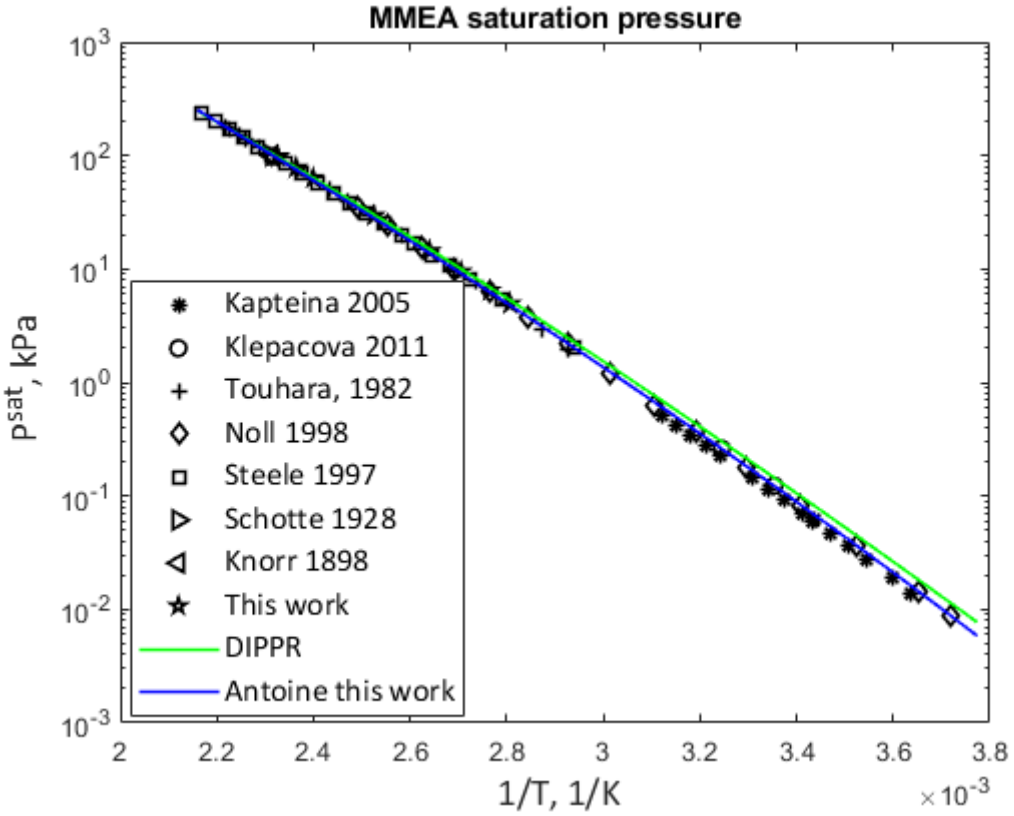

Figure 3. Model fit to available data for MMEA

The data from Kapteina et al. (2005) [43] were not used in the parameter fitting but are plotted in Figure 3. We see that, also for MMEA, the transpiration method seems to give slightly lower pressure values than the other sources. MMEA is more volatile than MDEA but

less volatile than DMMEA. The MMEA pressure values from this work, both as measured and corrected values, are given in Table A3 in the appendix. The correction was done in the same way as described for DMMEA using the water content given in Table 1. The Antoine fit to the data used in the fit had an AARD of 1.6 % and the data from Kapteina et al. (2005) [43] showed an AARD of 15.5%. The DIPPR [47] correlation can be seen to coincide with the developed Antoine equation at high temperatures but gives increasingly higher vapor pressure values at intermediate and lower temperatures.

3.1.4. AEP

Very little data was found for pure AEP. Data for the normal boiling point were found in several sources, mainly suppliers: Huntsman (2022) [50] , Sigma Aldrich (2022) [51] and from Parchem (2022) [49]. The normal boiling point was given as 220-224ºC and the value was relatively consistent between the suppliers. Some, Sigma Aldrich (2022) [51], Parchem (2022) [49] and Chemical databook (2022) [52], also give the saturation pressure at 20 or 25ºC, but there the scatter is larger. The only source of data over a more significant temperature span is from Efimova et al. (2010) [53], with 22 data points. These data are based on the transpiration method but were the only available data. The data used in the parameter fitting are listed in Table 5.

Table 5. Data used for regression of Antoine parameters for pure AEP.

Source	Data type	Data points
Huntsman (2022)[50]		1
Sigma Aldrich (2022) [51]		2
Parchem (2022) [54]		3
Chemical Databook (2022) [52]		1
Efimova (2010) [53]	Transpiration method	22

Model equations were provided by Efimova et al. [53], Stephenson and Malanowski [46], Yaws [55] and DIPPR [47] .

The fit to model is shown in Figure 4.

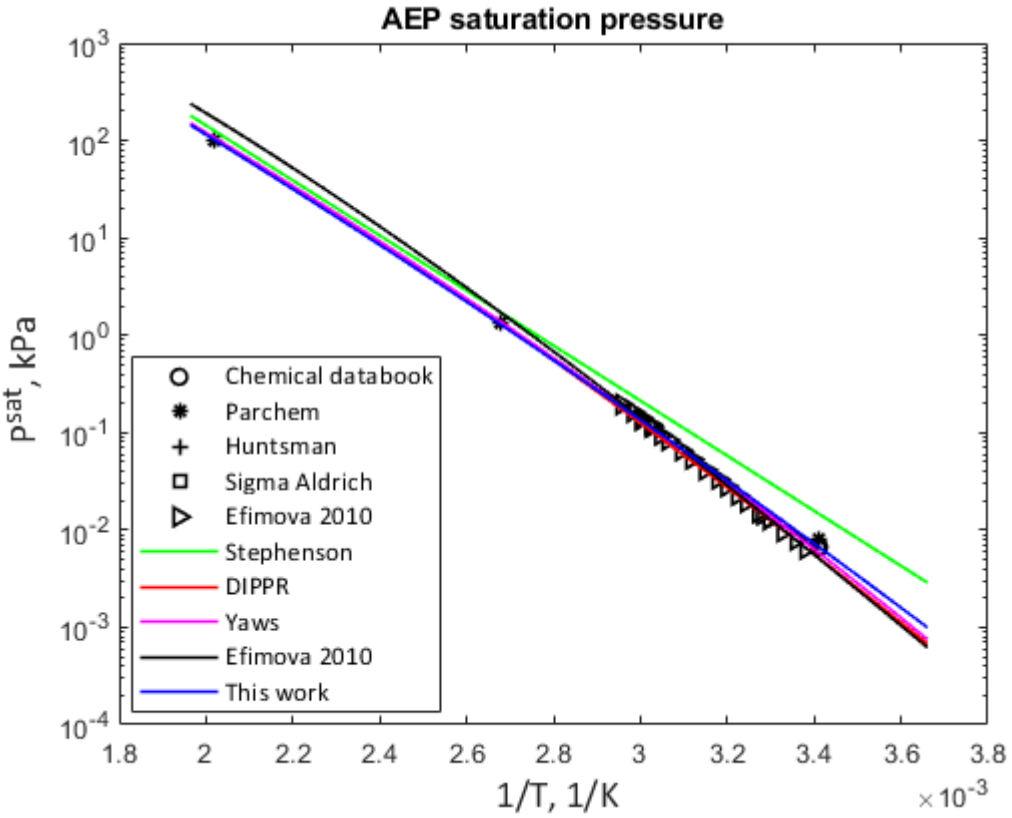

Figure 4. Model fit to available data for AEP

The AARD for the fitted Antoine equation compared to data is 2.2%. The developed equation almost coincides with the equation given by Yaws, et al. (2015) [55]. The DIPPR [47] equation predicts slightly lower saturation pressures in the intermediate temperature range but overpredicts the pressures at higher temperatures up to the normal boiling point. The equation given by Stephenson and Malanowski (1987) [46] overpredicts the pressure at intermediate and lower temperatures and should not be used.

In Table 6 are given the obtained Antoine parameters and the AARD's for the fits to all four components.

Table 6. Antoine parameters*

Component	A	B	C	AARD,%
MDEA	9.84	2111	-86.7	4.1
DMMEA	9.45	1520	-65.4	1.8
MMEA	10.13	1893	-63.8	1.6
AEP	10.04	2241	-50.0	2.2

* Psat in Pa and T in K.

3.2. Binary systems

3.2.1. MDEA-H_2O

Table 7 lists the data used in the NRTL parameter regression, while Table B1 in the appendix presents the VLE data from this work.

Table 7. Data used for regression of NRTL parameters for the MDEA-H2O system.

Source	Data type	Data points
This work	VLE (ebulliometer), $PTxy$	31
Kim et al. (2008) [16]	VLE (ebulliometer), $PTxy$	61
Xu et al. (1991) [56]	VLE (ebulliometer), PTx	34
Dell'Era et al. (2010) [32]	VLE (Static cell), PTx	31
Nguyen (2013) [57]	VLE (Static cell), $P_{Amine}Tx$	35
Kuwairi (1983) [58]	VLE (Static cell), PTx	20
Sidi-Boumedine et al. (2004) [59]	VLE (Static cell), PTx	4
Maham et al. (1997) [60]	Excess enthalpy, H^E	26
Posey et al. (1996) [61]	Excess enthalpy, H^E	17
Maham et al. (2000) [62]	Excess enthalpy, H^E	9
Mundwha and Henni (2007) [63]	Excess enthalpy, H^E	10

Isobaric data from Soames et al.(2018) [30] and Voutsas et al. (2004) [64], and the data from Na et al. [39], which were based on measured vapor phase compositions and calculated liquid phase compositions from a material balance, were not used in the model fit but compared with the model. The freezing point depression data from Fosbøl et al. (2011) [65] and Chang et al. (1993) [66] were also not used in the regression.

To obtain a good set of regressed NRTL parameters, both VLE and excess enthalpy data from the literature were part of the regression. Because excess enthalpies directly relate to the temperature dependence of the excess Gibbs energy, the inclusion of these data improves the temperature dependence of the model, see Posey (1996) [61].

Several ways of using the available experimental data for parameter fitting were tested. The VLE data from Xu et al. (1991) [56] and Dell'Era et al. (2010) [32], are PTx data. The data from Na et al. (2018) [39] are based on equilibrium obtained in vials with subsequent head space analyses performed with GC. The vapor compositions were determined by the ratio in peak area between the sample and pure MDEA. The details regarding how the peak areas were obtained are not given. In addition, the vapor composition values depend on the saturation pressure, which was earlier shown to be overestimated compared to other available data and the developed Antoine equation. Kim et al. (2008) [16] and data from this work contain vapor phase analyses based on LCMS-MS. The analytical method has high accuracy but obtaining a representative sample for the vapor phase is difficult because of the low volatility of MDEA. This gives a relatively high scatter in the data, but they were still used for parameter fitting since this work's main goal is to provide models that can predict amine volatility. Soames et al. (2018) [30] performed the Herington test for thermodynamic consistency of their data, see Wisniak (1994) [67] and Table 6 in Soames et al.(2018) [30]. A critical discussion on the appropriateness of this test is given by Van Ness (1995) [68] who advocates avoiding performing isobaric measurements altogether. Uncertainty about the isobaric data from Soames et al. (2018) [30] and Voutsas et al. (2004) [64] made us refrain from using these in the NRTL parameter fitting. Nguyen (2013) [57] provided partial pressure measurements for both MDEA and water and were used in the fit.

The excess heat of mixing data from Posey et al.(1996) [61], Maham et al. (1997, 2000) [60, 62], and Mundwha and Henni (2007)(57) were all used in the regression and improved the results. The FPD data from Fosbøl et al. (2011) [65] and Chang et al. (1993) [66] were used initially but were found to improve neither the overall fit nor the fit to the FPD data. They were thus excluded from the final fit.

Using, or not using, the PTx data from Xu et al. [56], Dell'Era et al. [32], Kuwairi (1983) [58] and Sidi-Boumedine et al. (2004) [59] was tested. No significant effect on the fit was observed and the data were included.

The regressed binary parameters for the system MDEA-H_2O are shown in Table 8, together with the parameters for the systems discussed later. For AEP, two fits are provided, 4A and 4B. 4B is a manually tuned version of 4A, see section 3.2.4 for further explanation.

Table 8. Regressed NRTL parameters for all binary systems.

System	Binary pair	a_{ij}	b_{ij}	α_{ij}
1	H_2O-MDEA	3.506	-822.8	0.919
	MDEA-H_2O	0.694	-449.0	0.919
2	H_2O-DMMEA	4.7313	-897.8	0.468
	DMMEA-H_2O	1.0953	-682.8	0.468
3	H_2O-MMEA	3.292	-60.74	0.274
	MMEA-H_2O	0.269	-763.1	0.274
4A	H_2O-AEP	-7.16	3579.1	0.866
	AEP-H_2O	-0.085	-482.1	0.866
4B	H_2O-AEP	-5.90	3515.0	0.571
	AEP-H_2O	-0.45	-482.1	0.571

Comparison with data

VLE

As we in this work focus on amine volatility, we have removed most of the total pressure figures to supplementary information. In Figure S1 in Supplementary information, the model fit to total pressure data from Kim et al. (2008) [16] and this work is shown. In Figure S1a),

the model is seen to overpredict the total pressure compared to data from Kim et al. [16], whereas the data from this work are seen to fit better to the model. In Figure S1b), the vapor phase data, both data from Kim et al. (2008) [16] and this work, are seen to be in good agreement with the model.

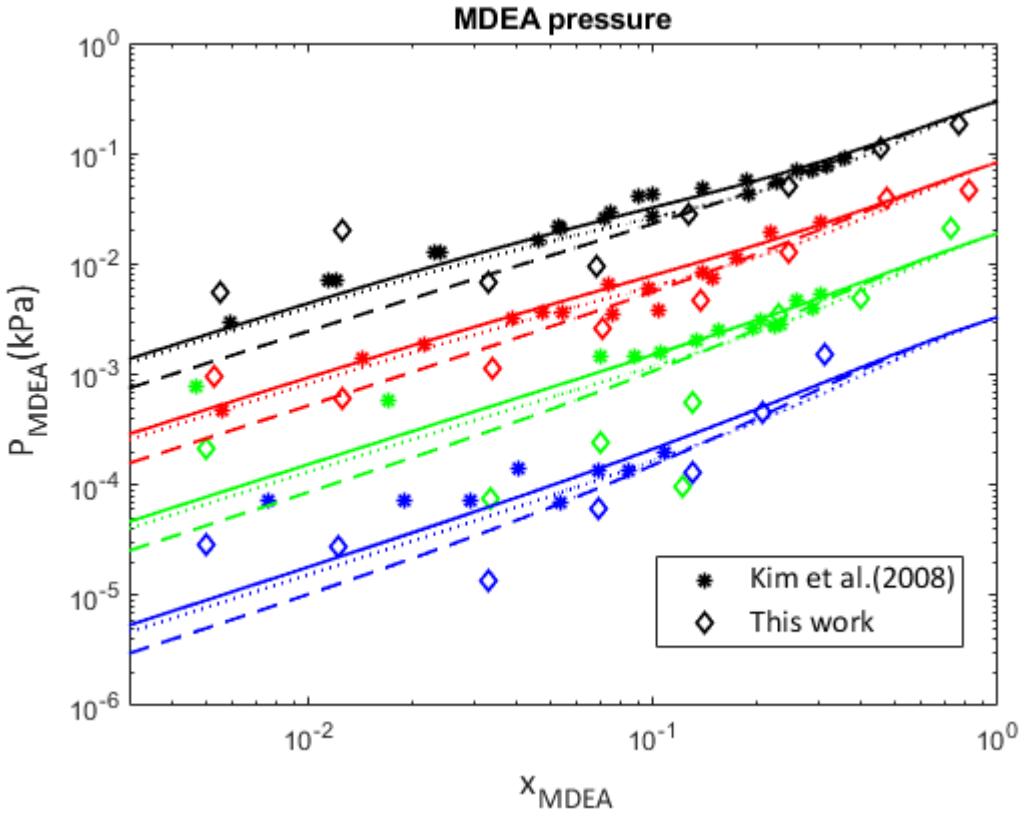

Figure 5. Calculated MDEA partial pressure plotted together with experimental data from this work and Kim et al. (2008) [16], Model: solid lines: This work, dashed lines: Schmidt et al. (2007)(24), dotted lines: Zhang and Chen(36). Blue: 40°C, green: 60°C, red: 80°C, black: 100°C.

Figure 5 shows predicted vapor pressures of MDEA compared with experimental data. As seen, the scatter in the data from this work is large. The reason for this is the low volatility of MDEA and thereby the difficulty in obtaining representative vapor phase samples. In spite of the large uncertainty in the vapor phase compositions, we have still included them in Table B1 and in Figure 5. A regression, only using PTx data, was performed and gave a fit

indistinguishable from the one based on the parameters given in Table 8. The model from this work is shown together with results using the models of Schmidt et al. (2007) (24) and Zhang and Chen (36). From the figure it is difficult to tell which model is the better because of the scatter in the data and the apparently small difference between the models. The difference between our model and the model of Schmidt et al. (2007) (24) increases with decreasing MDEA concentration, whereas the model by Zhang and Chen (2011) (36) follows the concentration trend of our model up to an MDEA mole fraction of about 0.2. Above this concentration level, the three models are very similar. It should be noted that 50 mass% MDEA, which is an industrial standard, corresponds to about 0.13 in mole fraction. In view of the data scatter, all three models represent the data reasonably well. As seen in Table 9, the AARD's for the fit to the P_{MDEA} data from Kim et al (2008) (16) are 23, 31 and 25% for the models from this work, Schmidt et al. (2007) (24) and Zhang and Chen (36) respectively.

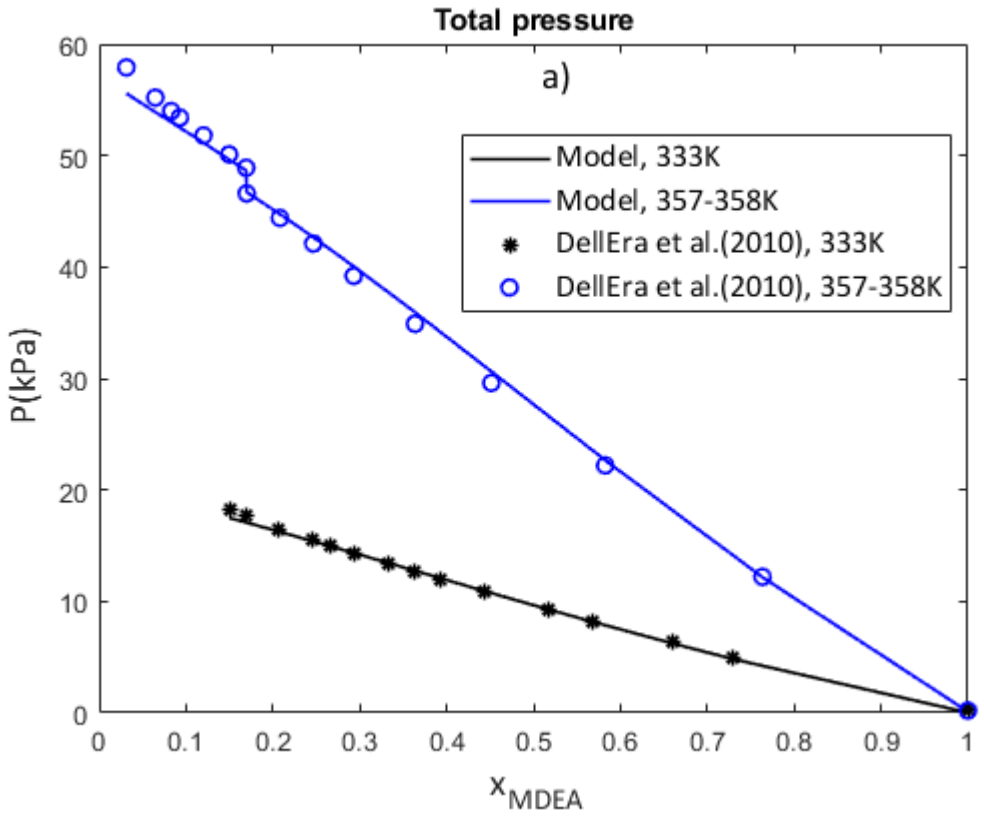

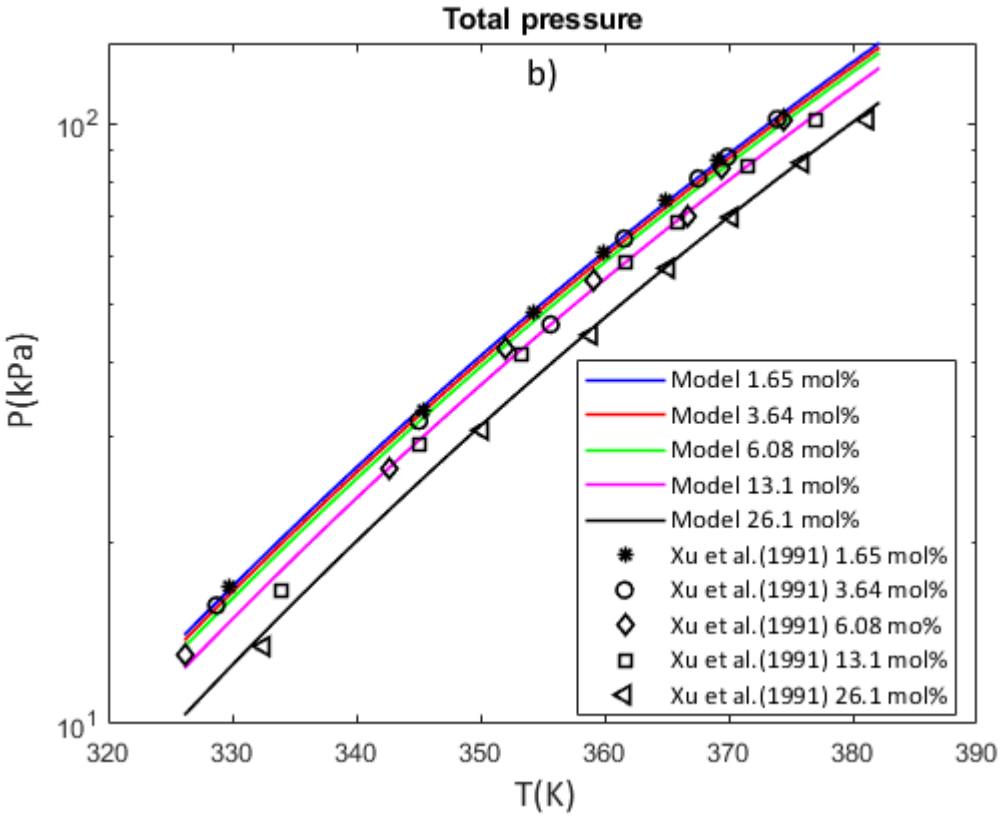
Total pressure
b)
P(kPa)
T(K)
Model 1.65 mol%
Model 3.64 mol%
Model 6.08 mol%
Model 13.1 mol%
Model 26.1 mol%
Xu et al.(1991) 1.65 mol%
Xu et al.(1991) 3.64 mol%
Xu et al.(1991) 6.08 mo%
Xu et al.(1991) 13.1 mol%
Xu et al.(1991) 26.1 mol%

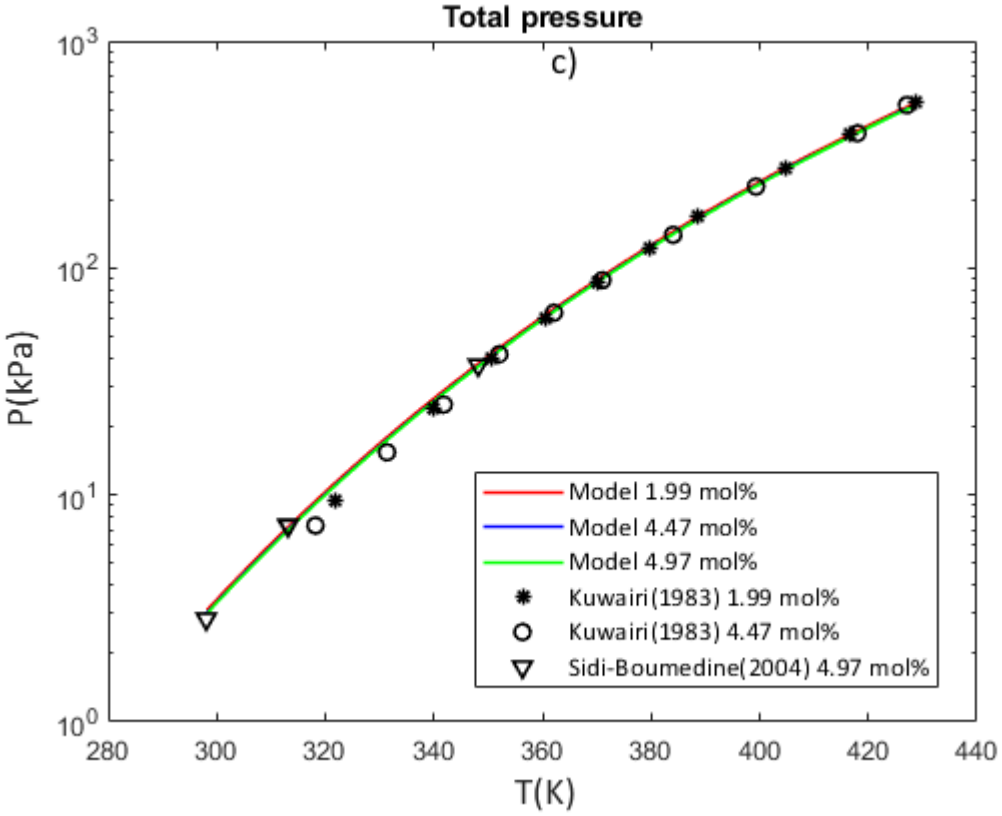
Total pressure
c)
P(kPa)
T(K)
Model 1.99 mol%
Model 4.47 mol%
Model 4.97 mol%
Kuwairi(1983) 1.99 mol%
Kuwairi(1983) 4.47 mol%
Sidi-Boumedine(2004) 4.97 mol%

Figure 6. Calculated total pressure from the model in this work, plotted together with experimental data from: a). Dell'Era et al. (2010) [32], b). Xu et al. (1991) [56] and c). Kuwairi (1983) [58] and Sidi-Boumedine et al. (2004) [59]

The present model fit to data from Dell'Era et al. (2010) [32], shown in Figure 6a), is good at both temperatures given, apart from at the high temperature and lowest amine concentrations. Likewise, the model agreement with data from both Xu et al. (1991) [56], Kuwairi (1983) [58] and Sidi-Boumedine et al. (2004) [59] is excellent, as seen from Figure 6b) and 6c). Xu et al. (1991) [56] note that the maximum relative deviation in their data from Raoult's law was 9.1% and the absolute average error 2.2%, and concluded that Raoult's law can be used for the MDEA/water system. This may be true if total pressure were the only objective. However, when continuing to systems involving CO_2, both the MDEA and water activities and volatilities are important variables to establish good ternary equilibrium and kinetic models and to enable reasonable predictions of MDEA emissions. For this purpose, a more accurate model is needed.

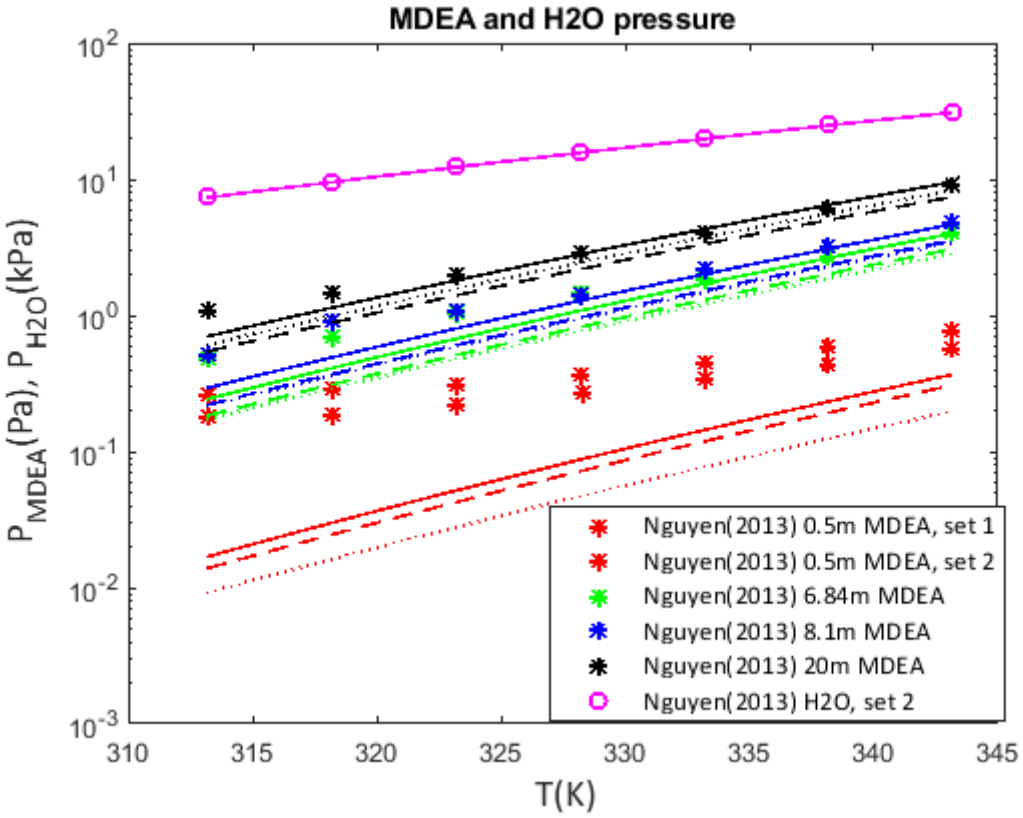

Figure 7. Predicted and experimental amine and water pressures, Experimental data from Nguyen [57] Model: solid lines this work, dashed lines Zhang and Chen (36), dotted lines Schmidt et al (2007)(24). Red: 0.5m MDEA, green: 6.84m MDEA, blue: 8.1m MDEA and black: 20m MDEA, mauve: water pressure in 0.5m MDEA.

In Figure 7 the amine and water pressure data from Nguyen (2013) [57] are given and compared with model predictions from this work and from using the NRTL parameters of Zhang and Chen (2011) (36) and Schmidt et al (2007)(24). The temperature trends of the three models are almost the same, but the parameters from Zhang and Chen (2011) (36) predict MDEA partial pressures about 30% lower than the model from this work at all concentrations. The parameters of Schmidt et al., (2007) (24) are seen to predict MDEA partial pressures about half of the model from this work at the lowest MDEA concentration. At higher MDEA concentrations, the difference between The Schmidt et al., (2007) (24) model and the present one decreases, and for 20m MDEA it is about 17%. The model predictions from this work agree well with experimental data at higher temperatures but deviate in the low range for the

three highest amine concentrations. At the lowest amine concentration, predictions are much lower than the experimental values for all three models. Nguyen (2013) [57] gives two data sets at the lowest amine concentration which deviate from each other. The gas phase analyses were performed using FTIR, and the detection limit was given as 1 ppm (0.1Pa), indicating that values in the low ppm range will have high uncertainty.

In the Supplementary information, Figure S2, are shown comparisons between model predictions and data from Na et al. (2018) [39], Soames et al. (2018) [30] and Voutsas et al.(2004) [64]. These data sets were not used in the parameter fit. In Figure S2 a) it is seen that the model is not able to represent the Na et al. (2018) [39] data well. Na et al. (2018) [39] give an analytical uncertainty in the vapor mole fraction of ±0.001. Most of the MDEA vapor mole fractions are below 0.004, possibly resulting in high uncertainty. The liquid phase compositions were calculated from the gas phase compositions using the saturation pressure relationship given in Figure 1, which was shown to overestimate the MDEA pressure. We therefore deem the uncertainty of these data to be significant. Figure S2 b) shows excellent agreement between the model and data from Soames et al. (2018) [30], and in Figure S2 c), the agreement with data from Voutsas et al. (2004) [64] is also seen to be good for MDEA mole fractions below 0.75.

In Figure S3 in Supplementary information, the model fit to experimental activities calculated from the data of Kim et al. (2008) [16] and from this work is given. The water activities predicted by the model are higher than the data from Kim et al. (2008) [16] but fit better to the data from this work, see Figure S3 b). The MDEA activities are reasonably well predicted compared both to data from Kim et al. (2008) [16] and this work, see Figure S3 a). However, the activity coefficient data show high scatter both for water and MDEA. In Figure S3 are also plotted curves based on the NRTL model of Schmidt et al. (2007) (24). This model

is seen to under-predict the MDEA activity coefficients, in particular at low amine concentrations. Also, the water activity coefficients are lower than data from Kim et al (2008) (16) and from this work. It should be noted that the deviations in water activity coefficient are within 5-10%, whereas for MDEA, they are up to 50-80%.

As seen in the Supplementary Information Figure S4, the model from this work does not to describe activity coefficients calculated from the data of Na et al. (2018) [39] satisfactorily. This is expected based on the discussion given earlier. The NRTL model by Schmidt et al. (2007) is also seen to deviate from the data of Na et al. (2018) [39].

Freezing point depression and enthalpy of mixing

The model results for freezing point depression are shown in Figure 8a) together with literature data from Fosbøl et al. (2011) [65] and Chang et al. (1993) [66]. The method used for calculating the freezing point depression is according to Ge and Wang (2009) [69] and Prausnitz et al. (1999) [23]. As given in Table 9, the AARD's for the freezing point depression predictions were calculated to 3.6% compared to data from Fosbøl et al. (2011) [65] and 10.2% compared to data from Chang et al. (1993) [66]. This indicates a good fit between the model and experimental data even though these data were not used in the regression. Over the whole concentration range, the data from Fosbøl et al. (2011) [65] seem to be more consistent with the modelled results. We have also included model results using the NRTL parameters from Zhang and Chen (2011) (36), which are seen to underestimate the freezing point depression at higher MDEA concentrations.

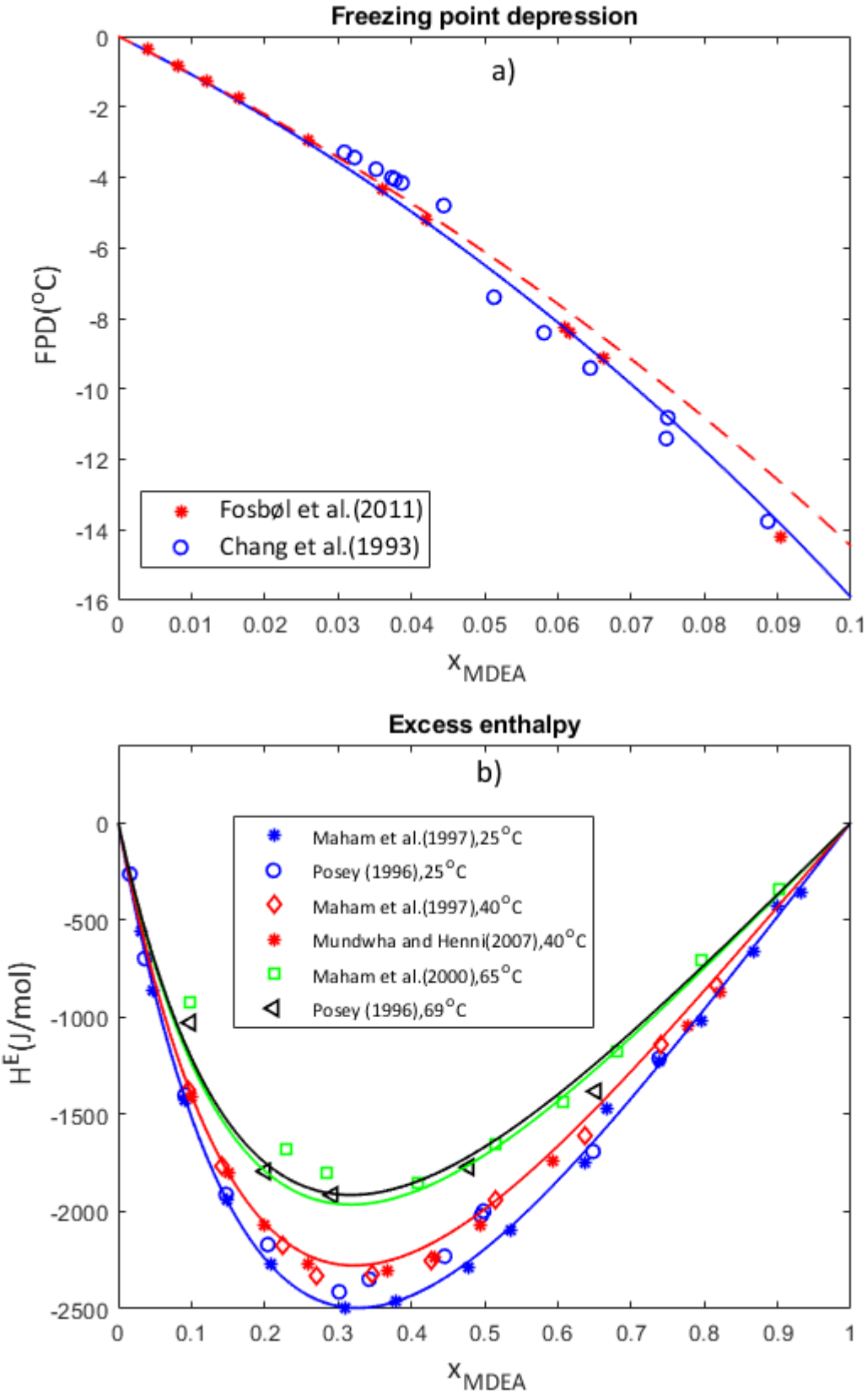
Freezing point depression
a)
FPD(°C)
0
-2
-4
-6
-8
-10
-12
-14
-16
0
0.01
0.02
0.03
0.04
0.05
0.06
0.07
0.08
0.09
0.1
x MDEA
Fosbøl et al.(2011)
Chang et al.(1993)
Excess enthalpy
b)
H E (J/mol)
0
-500
-1000
-1500
-2000
-2500
0
0.1
0.2
0.3
0.4
0.5
0.6
0.7
0.8
0.9
1
x MDEA
Maham et al.(1997),25 °C
Posey (1996),25 °C
Maham et al.(1997),40 °C
Mundwha and Henni(2007),40 °C
Maham et al.(2000),65 °C
Posey (1996),69 °C

Figure 8. a) Calculated freezing point depression together with literature data from Fosbøl et al. (2011) [65] and Chang et al. (1993) [66], model: solid line this work, dashed line Zhang and Chen (2011)(36), b) Calculated excess enthalpies at 25, 40, 65 and 69.4°C plotted together with literature data, Posey et al. (1996), Maham et al. (1997, 2000) [60, 62] and Mundwha and Henni(2007) [70] . Model lines: this work, blue: 25°C, red: 40oC, green: 65°C and black: 69.4°C.

Calculated excess enthalpies and experimental data from Maham et al. (1997, 2000) [60, 62], Posey (1996) [61] and Mundwha and Henni(2007) [70] at various temperatures are shown in figure 8b). The model fit to the Maham et al. (1997) [60] data at 25 and 40°C is excellent with an AARD of 2.9%. The fit to data by Posey et al. (1996) [61] is reasonable with an AARD of 5.9%. At 40°C, the model predicts a little lower values than the data from Maham et al. (2000) [62], with an AARD of 8%, and for the data from Mundwha and Henni (2007) [70], with an AARD of 3.5%. It should be noted that the scatter in the data is significant and that the measurements by Maham et al. (2000) [62] at 69.4°C lie above those of Posey et al. (1996) [61] at 65°C. The opposite would be expected.

In Supporting Information Figures S5 (a-d) are given comparisons between several NRTL models and the existing data at individual temperatures. The models tested are from Posey et al. (1996) [61], Schmidt et al. (2007) [24], Kim et al. (2008) [16] and this work. At the highest temperatures, the models of Posey et al. (1996) [61] and Kim et al. (2008) [16] over-estimate the magnitude of the excess heat, with Kim et al. (2008) [16] giving the highest values. The models from Schmidt et al. (2007) [24] and this work give very similar results close to the experimental values.

Specific heat.

The Cp for the water/MDEA mixtures was calculated from the NRTL model and compared to data from Hayden and Mather (1983) [71] and Chen et al. (2001) [72] with AARD's of 3.2 and 2.3%, respectively. The model used for Cp for pure MDEA was taken from Shokouhi et

al. (2013) [73]. Two other Cp-models for pure MDEA, from Chen et al. (2001) [72] and Maham et al. (1997) [60] were also tested and gave slightly higher Cp values for the mixtures. The comparisons are shown in Figure S6 in Supporting Information.

Agreement with the various data sources.

In Table 9, the AARD's for the agreement between the model and the various experimental sources is given. The figures range from excellent to reasonable for all variables apart from the vapor phase MDEA concentrations. The inconsistency between measured and predicted vapor phase concentrations is believed to be primarily an experimental problem caused by difficulties in obtaining representative vapor phase samples. Again, this points to the need for better vapor phase data for the water/MDEA system. Both Schmidt et al. (2007) [24] and Zhang and Chen (2011) (36) discussed the use of the NRTL model for MDEA/water thoroughly and deduced sets of NRTL parameters for the system. The fit to their parameters is also included in Table 9. The parameters from Schmidt et al. (24) give a somewhat better fit to vapor phase compositions from the present work and to the data from Na et al. (2018) [39]. However, the fit to MDEA activity coefficients, as discussed earlier, is better in the present model. This results in a significantly better fit to the MDEA volatility data given by both Kim et al. (2008) (16) and Nguyen (2013) [57]. Using parameters from Zhang and Chen (2011) (36) gives a similar fit to the vapor composition data from Na et al. (2018) (37), but gives larger deviations for most other data, and in particular for the MDEA partial pressure data from Nguyen (2013) (55).

Table 9. AARD's for the model fit to experimental data

Data type	Source	Variable	AARD	AARD[#]	AARD[##]
$PTxy$	This work	P_T	5.6%	8%	7.5%
		P_{MDEA}	166%	105%	123%
$PTxy$	Kim et al. (2008) [16]	P_T	1.6%	0.7%	1.9%

		P_{MDEA}	23%	31%	25%
$PTxy$	Na et al. (2018) [39]	P_T	6.2%	3.6%	6.3%
		y_{MDEA}	44.9%	17.4%	30.5%
$PTxy$	Soames et al. (2018) [30]	$T(K)$	0.4%	0.7%	1.2%
		y_{MDEA}	16%	25%	38%
PTx	Voustas et al. (2004) [64]	$T(K)$	1.0%	0.9%	0.6%
PTx	Xu et al. (1991) [56]	P_T	2.2%	2.4%	2.5%
PTx	Kuwairi (1983) [58]	P_T	5.4%	5.2%	5.4%
PTx	Sidi-Boumedine et al. (2004) [59]	P_T	3.9%	4.1%	3.9%
PTx	Dell'Era et al. (2010) [32]	P_T	5.8%	11%	8.5%
PTx	Nguyen (2013) [57]	P_{MDEA}	19%*	36.2%*	37%*
H^E	Maham, et al. (1997) [60]	H^E	2.9%	5.1%	5.4%
H^E	Maham, et al. (2000) [62]	H^E	8.0%	7.2%	11.2%
H^E	Posey (1996) [61]	H^E	5.9%	5.8%	6.4%
H^E	Mundwha and Henni (2007) [70]	H^E	3.5%	5.8%	4.7%
FPD	Fosbøl,et al. (2011) [65]	FPD	3.6%	5.9%	5.4%
FPD	Chang et al. (1993) [66]	FPD	10.1%	11.1%	10.4%
Cp	Chen et al. (2001) [72]	Cp	2.3%	2.0%	1.3%
Cp	Hayden et al. (1983) [71]	Cp	3.2%	1.4%	1.9%

*Not included the lowest MDEA concentration. #Using parameters from Schmidt et al. (2007) [24].
##Using parameters from Zhang and Chen (2011) (36)

3.2.2. DMMEA-H_2O

For the DMMEA-water system, three VLE literature references were found: Touhara et al. (1982) [36], Chiali-Baba-Ahmed et al. (2013) [41] and Nguyen (2013) [57]. The two first provide only PTx data, although Chiali-Baba-Ahmed et al. (2013) [41] give calculated vapor compositions. Nguyen (2013) [57] provides partial pressure data for both water and DMMEA. In addition, freezing point depression data are given by Chang et al. (1993) [66], and excess heat of mixing data by Mundhwa and Henni (2007) [63]. The data used for fitting the binary NRTL parameters are given in Table 10.

Table 10. Available data for the DMMEA-H_2O system.

Source	Data type	Data points
This work	VLE (Ebulliometer), $PTxy$	21
Chiali-Baba-Ahmed et al. (2013) [41]	VLE (Static cell), PTx	90
Touhara et al. (1982) [36]	VLE (Static cell), PTx	32

Nguyen (2013) [57]	VLE (Static cell), $P_{DMMEA}Tx$	7
Touhara et al. (1982) [36]	Excess Enthalpy, H^E	41
Mundhwa and Henni (2007) [63]	Excess Enthalpy, H^E	36
Chang et al. (1993) (63)	Freezing point depression	26
Mundhwa (2007) (67)	Specific heat, Cp	111

Except the Cp data from Mundhwa (2007) (67) and the freezing point depression data from Chang et al. (1993) (63), all data in Table 10 were used in the parameter regression. Including the freezing point depression data had a small negative effect on the resulting fit to the other data without significantly improving the fit to the FPD data. The regressed parameters in the NRTL model are given in Table 8 and AARDs for the various data sets are shown in Table 11.

Comparison with data

VLE

The total pressure data from this work, tabulated in Appendix B, Table B2, compared with model results, are shown in Supplementary information Figure S7. They cover DMMEA concentrations up to about 0. 23 in liquid phase mole fraction, equivalent to 0.49 in mass fraction. The liquid phase data are well represented by the model with an AARD of 0.3% in total pressure, whereas the gas phase data at the highest temperatures deviate somewhat from the model, resulting in an AARD of 14.3%.

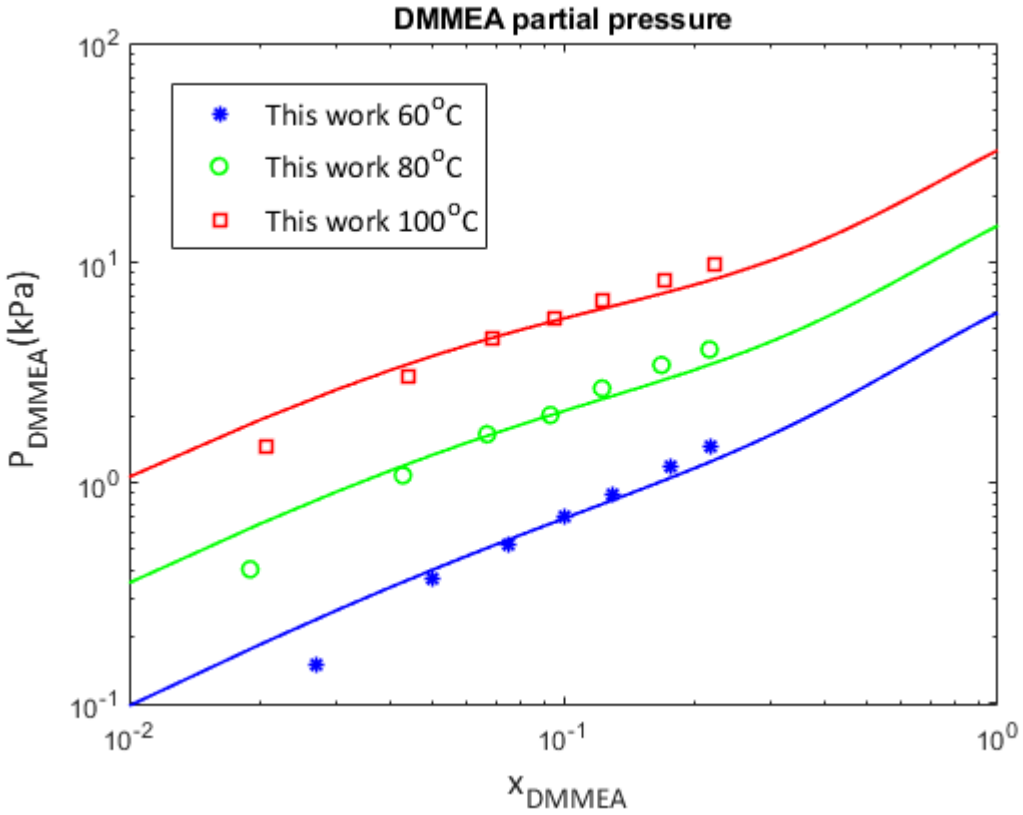

Figure 9. Calculated partial pressure of DMMEA compared with experimental data from this work.

In Figure 9, the experimental and predicted partial pressures of DMMEA are compared. The model slightly under-predicts the partial pressures above 0.1 in mole fraction, but the deviations are, for all points apart from the three points at the lowest concentrations, below 15%. This is about the estimated aggregate experimental uncertainty in P_{DMMEA}. In Figure 10, the model is compared with data from Nguyen (2013) (55) at a mole fraction of 0.01 and shows excellent agreement with the data through the whole temperature range with an AARD of 1.3% for P_{DMMEA} and 4.4% for P_{water}. This may indicate that the apparent over-predictions at the lowest DMMEA concentrations in Figure 9 could be caused experimental uncertainty.

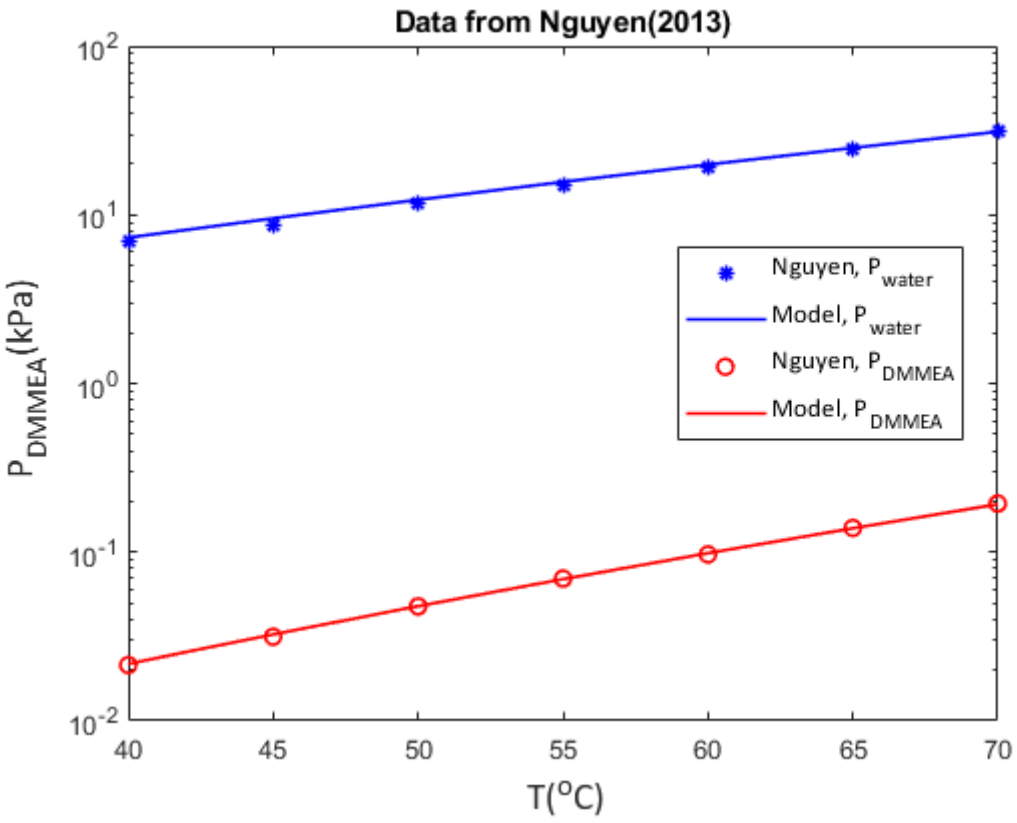

Figure 10. Calculated partial pressure of DMMEA and water compared with experimental data from Nguyen (2013) [57].

Figure 11 a) and b) show comparisons between data from Chiali-Baba-Ahmed et al. (2013) [41] and model predictions. The agreement is excellent throughout most of the concentration range, but slight underpredictions are seen above a DMMEA mole fraction of about 0.7. The overall AARD was found to be 3.1% for total pressure versus liquid phase composition and 7% for the vapor phase composition.

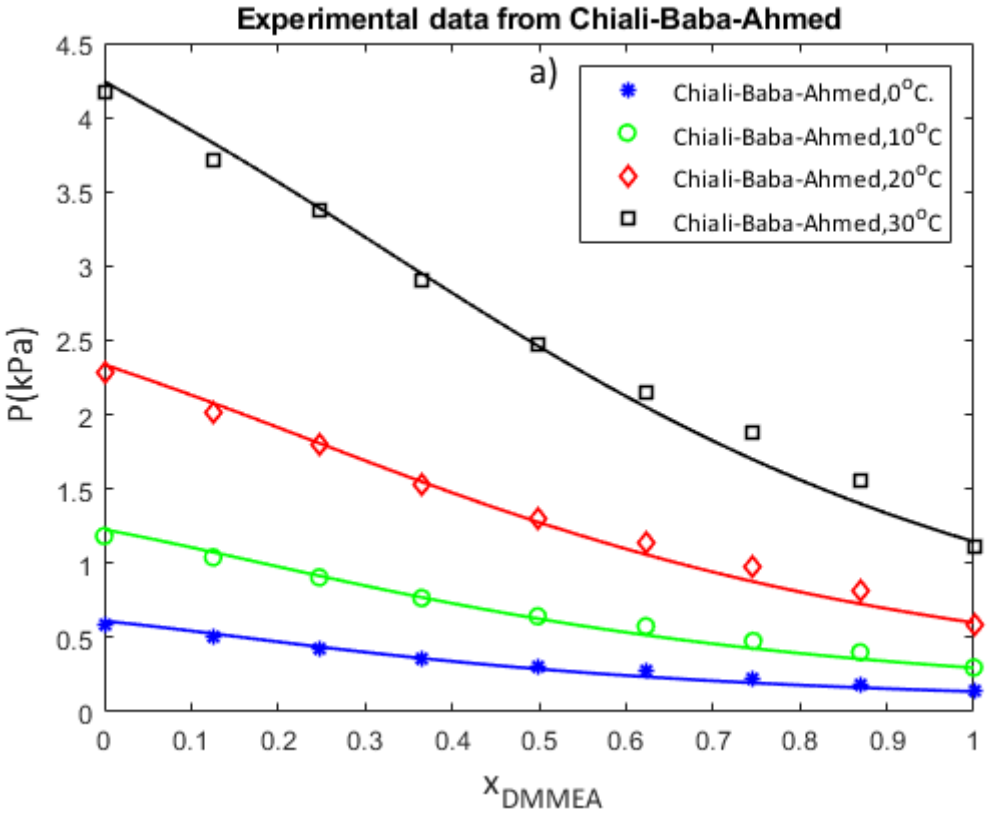
Experimental data from Chiali-Baba-Ahmed
a)
Chiali-Baba-Ahmed,0°C.
Chiali-Baba-Ahmed,10°C
Chiali-Baba-Ahmed,20°C
Chiali-Baba-Ahmed,30°C
P(kPa)
x DMMEA

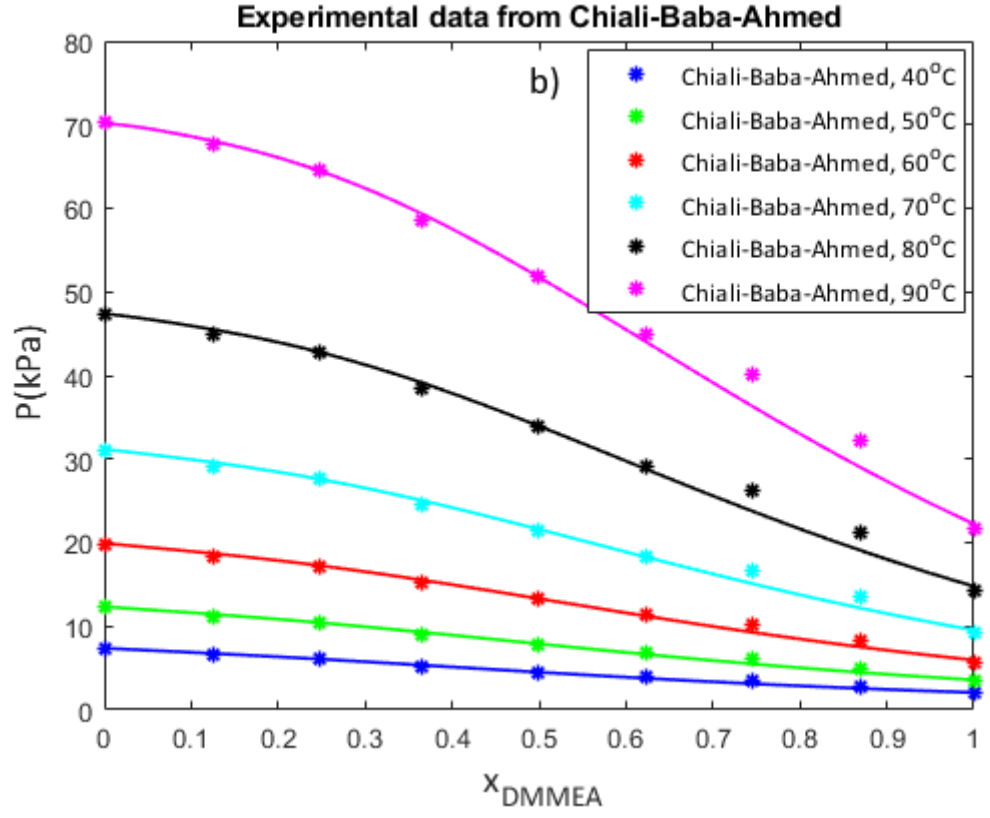
Experimental data from Chiali-Baba-Ahmed
b)
Chiali-Baba-Ahmed, 40°C
Chiali-Baba-Ahmed, 50°C
Chiali-Baba-Ahmed, 60°C
Chiali-Baba-Ahmed, 70°C
Chiali-Baba-Ahmed, 80°C
Chiali-Baba-Ahmed, 90°C
P(kPa)
x DMMEA

Figure 11 a). and b). Calculated total pressure from the NRTL model compared with experimental data at 273 to 363 K from Chiali-Baba_Ahmed et al. (2013) [41]. Lines from model in this work.

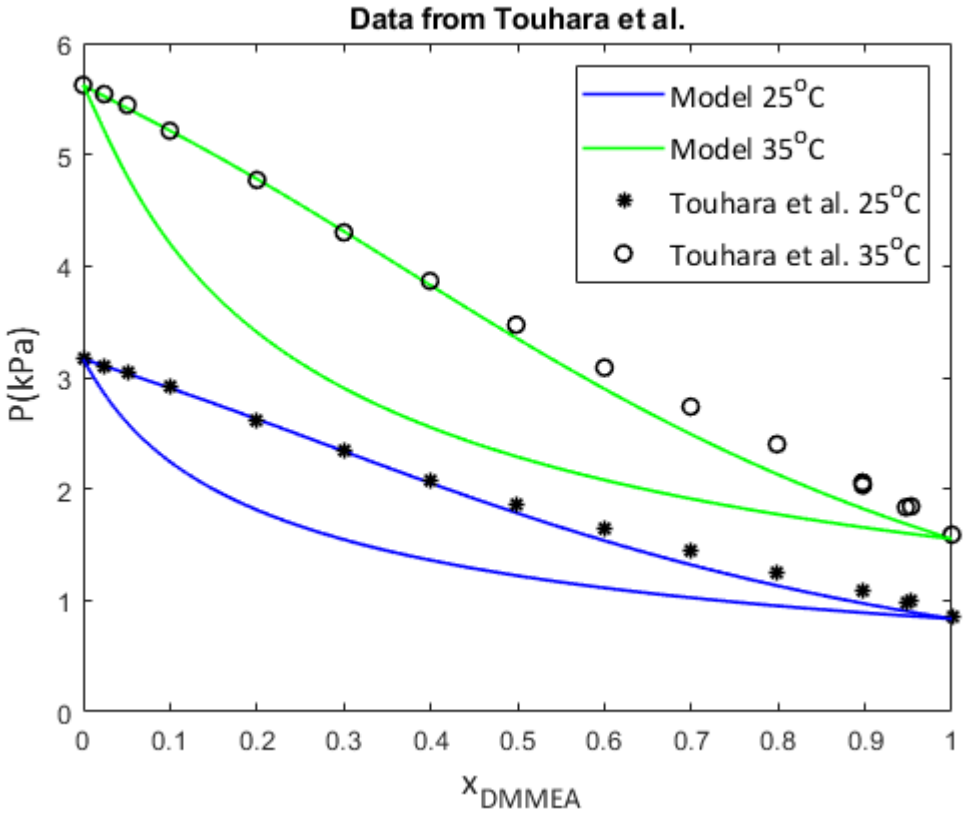

Figure 12. Calculated total pressure plotted together with experimental data from Touhara et al. (1982) [36].

In Figure 12, comparisons between data from Touhara et al. (1982) [36] and the model in this work are shown. Also, for the data from Touhara et al. (1982) [36] the agreement is good, but small deviations occur at mole fractions above 0.6 giving an AARD of 3.6%.

In Figure S8 a) in the Supplementary information, the DMMEA activity coefficients from this work are calculated and compared with model predictions. As for MDEA, the uncertainty in the gas phase concentrations is significant, although, since DMMEA is more volatile, the gas phase concentrations are higher in this case, making the accuracy better than for MDEA.

The model predicts the trends in the experimental DMMEA activity data reasonably well and the water activities agree very well with model predictions.

In Figure S8 b), activity coefficients at 0, 40 and 90°C are calculated based on the vapor compositions given by Chiali-Baba-Ahmed et al. (2013) [41] and compared with model predictions. Up to DMMEA mole fractions of about 0.5, the calculated and model activities for both DMMEA and water agree well. At higher concentrations, the calculated activities deviate from the experimental ones. However, the experimental DMMEA activities show significant scatter in this range.

In Figure 13 a), the model predicted excess enthalpies of mixing are compared with experimental data from Mundhwa and Henni (2007) [63] and Touhara et al. [36]. The agreement is seen to be very good for the lowest temperature with an AARD of 2.5% for the data from Touhara et al. (34). For the data from Mundhwa and Henni (2007) (71), the fit is also good with an AARD of 3.9% for all temperatures combined. Even if the discrepancies at 60°C seem large, we believe they are within experimental uncertainty.

Figure 13 b) shows the model predicted freezing point depressions compared with experimental data from Chang et al. (1993) [66], using the model by Ge and Wang (2009) [69] and Prausnitz et al. (1999) [23]. Even though the FPD data were not used in the parameter fitting, the agreement between the model and experimental data is still good, with an AARD of 1.4%.

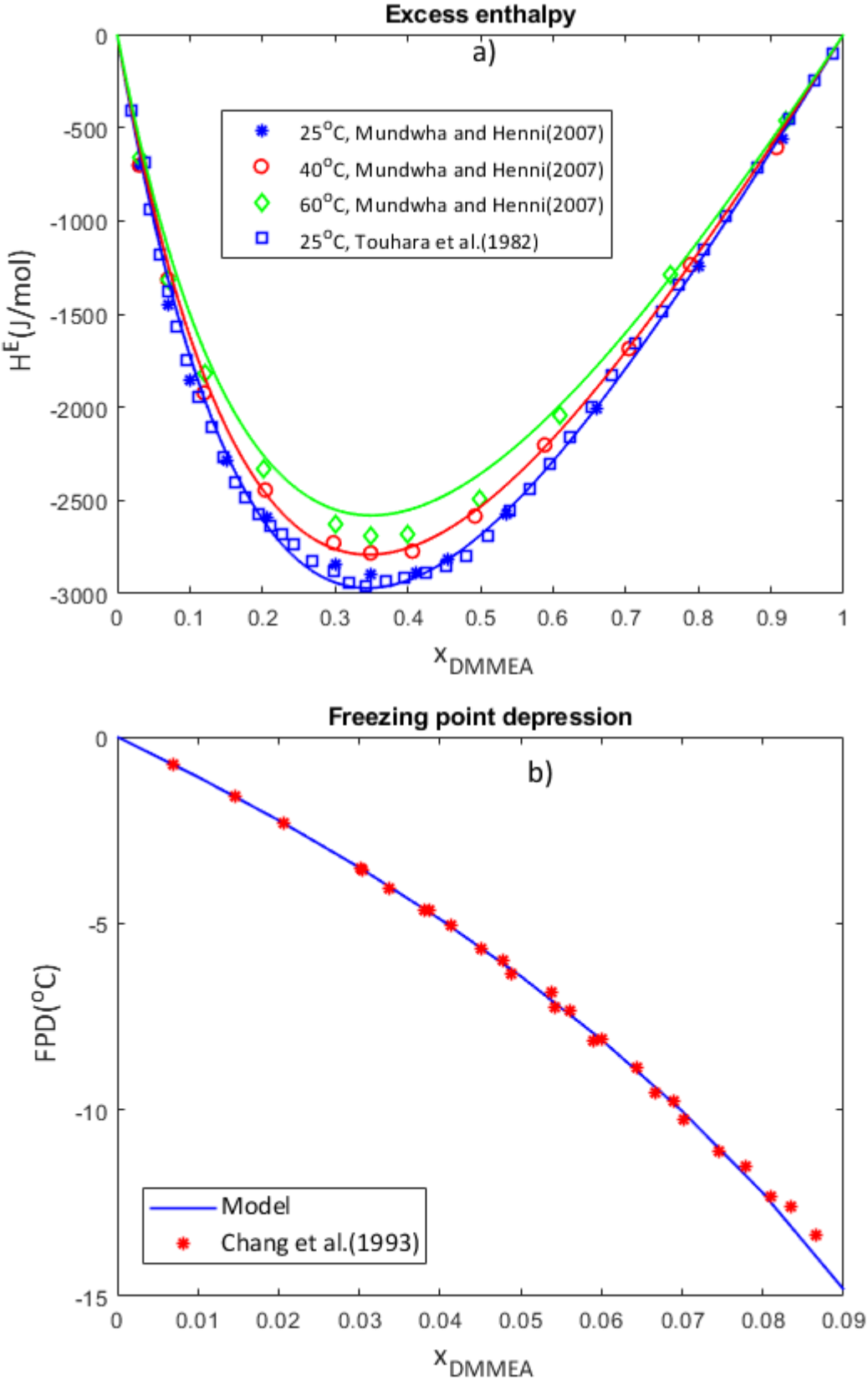
Excess enthalpy
a)
25°C, Mundwha and Henni(2007)
40°C, Mundwha and Henni(2007)
60°C, Mundwha and Henni(2007)
25°C, Touhara et al.(1982)
H^E(J/mol)
x_DMMEA
Freezing point depression
b)
Model
Chang et al.(1993)
FPD(°C)
x_DMMEA

Figure 13 a): Experimental excess enthalpy data from Mundhwa and Henni (2007) [63] and b): FPD for DMMEA-water from Chang et al. (1993) [66] compared with NRTL model calculations.

Specific heat.

In Figure S9, in supplementary information, the agreement between modelled and experimental specific heat values for DMMEA/water is shown. Experimental data are taken from Mundhwa (2007) (67), and the predictions, given by lines, are based on a Cp model for pure DMMEA from Mundhwa and Henni (2007) (71). The agreement between the model and experimental data is not good, but the model shows reasonable trends. The predictions are good for the lowest temperatures for all mole fractions. There is a strong increase in experimental Cp with temperature shown by neither pure water nor DMMEA. This leads the experimental values for a DMMEA mole fraction of 0.9 to exceed the curve for pure DMMEA at the highest temperature.

Agreement with the various data sources.

In Table 11 are given the AARD values, and as seen, the agreement is generally very good. The vapor phase compositions are also well represented and much better than for MDEA. The reason for this is the higher volatility of DMMEA, making the experimental work more accurate. However, it is still much higher than the rest of the AARD's in Table 11 because of the higher experimental uncertainty for vapor phase measurements.

Table 11. AARD's for the various data sets.

Data type	Source	Variable	AARD
$PTxy$	This work	P_T	0.3%
$PTxy$	This work	P_{DMMEA}	14.3%
PTx	Chiali-Baba-Ahmed et al. (2013) [41]	P_T	3.9%
PTx	Touhara, et al. (1982) [36]	P_T	4.5%
$PTxy$	Nguyen (2013) [57]	P_{DMMEA}	1.3%
H^E	Mundhwa and Henni (2007) [63]	H^E	3.9%

H^E	Touhara et al. (1982) [36]	H^E	2.5%
FPD	Chang et al. (1993) [66]	FPD	1.4%
Cp	Mundhwa (2007) [63]	Cp	8.4%

3.2.3. MMEA-H_2O

The only set of binary VLE data found in the literature for MMEA/water was from Touhara et al. (1982) [36]. Both Touhara et al. [36] and Mundhwa and Henni [63] provide excess enthalpy data.

Table 12. Available data for the MMEA-H_2O system.

Source	Data type	Data points
This work	VLE (Ebulliometer), $PTxy$	52
Touhara et al. (1982) [36]	VLE (Static cell), PTx	26
Mundhwa and Henni (2007) [63]	Excess enthalpy, H^E	43
Touhara et al. (1982) [36]	Excess enthalpy, H^E	43
Mundhwa (2007) (67)	Specific heat, Cp	111

The Cp data found in Mundhwa (2007) (67) were not used in the parameter regression. No freezing point depression data were found and all other available data in Table 12 were used in the regression of NRTL parameters.

The regressed parameters in the NRTL model are given in Table 8, and AARDs for the various data sets are shown in Table 13.

Comparison with data

VLE

Figure S10 in the supplementary information shows the comparison between experimental total pressure data from this work and the NRTL model. The agreement is excellent, with AARD's for total pressure and vapor mole fraction of 0.5 and 6.8% respectively. The data from Touhara et al. (1982) [36] cover the whole concentration range, and together with the data from this work, the model covers the temperature range 25 to 100°C.

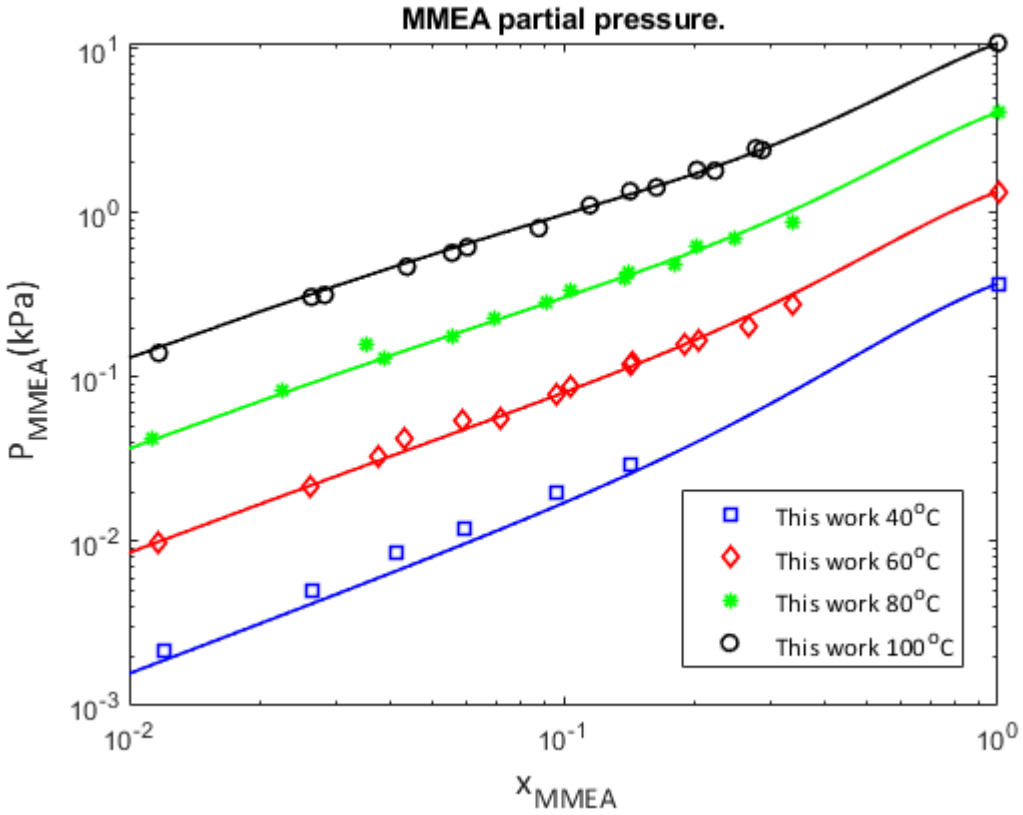

Figure 14. Model fit to experimental MMEA partial pressure data from this work. Model: blue: 40°C, red: 60°C, green: 80°C and black: 100°C.

Figure 14 shows the comparison between experimental and predicted MMEA partial pressures from this work. The agreement is very good, and, apart from one point, within 20%. The overall AARD is 7.3%.

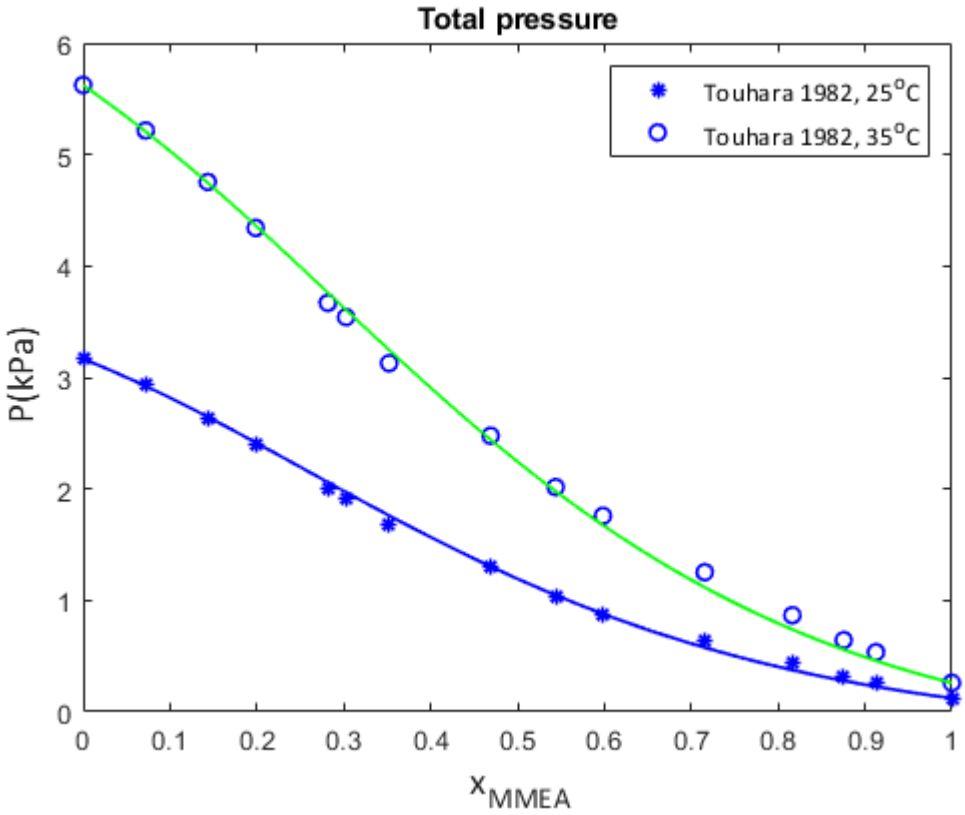

Figure 15. Model fit to experimental total pressure data from Touhara et al.(1982) [36]. Model: blue: 25ºC, green: 35ºC.

Figure 15 shows the model fit to total pressure data from Touhara et al. (1982) (34). The fit is excellent in the whole concentration range with and AARD of 4.6%.

Figure S11 in the supplementary information shows the experimental and calculated activity coefficients from this work. The scatter in the experimental data for MMEA is not so large as for MDEA, but still considerable for the lower temperatures. The model fit for water activity is good and for MMEA it is deemed satisfactory.

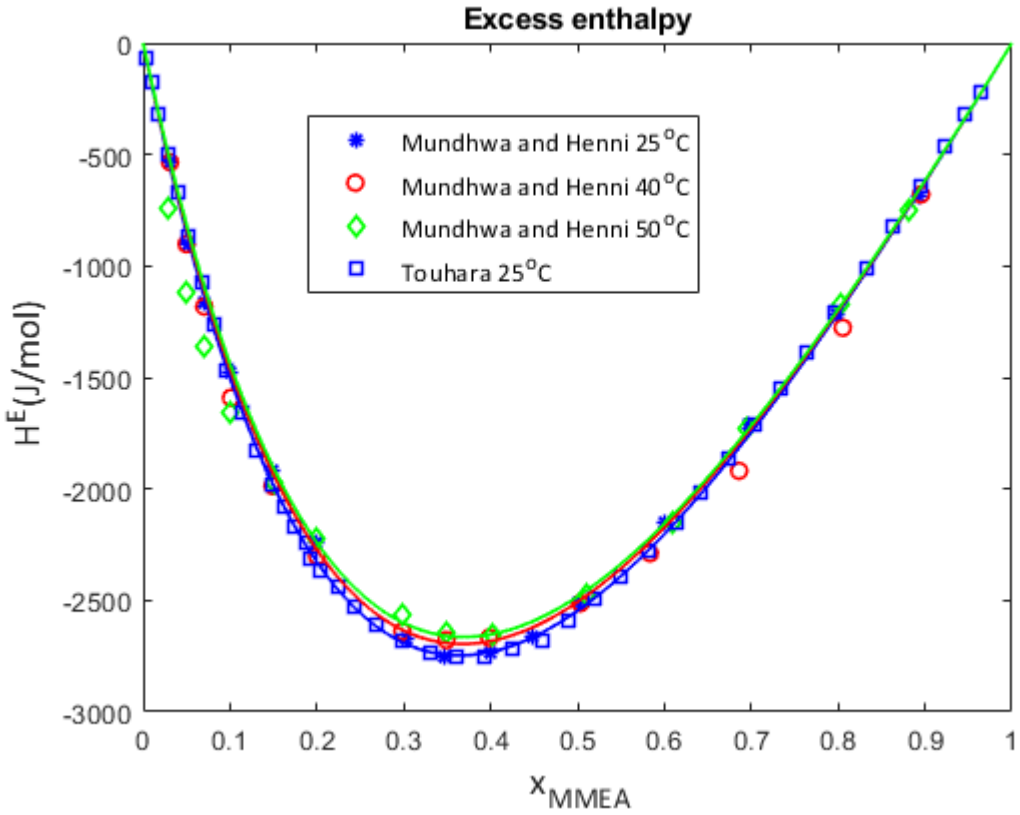

Figure 16. Excess enthalpy data from Touhara et al. (1982) [36] and Mundhwa and Henni (2007) [70] compared to model predictions.

Figure 16 gives a comparison between experimental and modelled excess enthalpies of mixing. The agreement is excellent with AARDs of 1.5 and 4.2% compared to data from Touhara et al. (1982) (34) and Mundhwa and Henni (2007) (71) respectively.

Specific heat.

Predicted Cp values for aqueous MMEA compared with experimental data from Mundhwa (2007) (67) for both pure MMEA and aqueous blends are shown in supplementary information Figure S12. As for DMMEA, the agreement between model and experimental data is good at 30°C, but also for MMEA the experimental data show a strong increase with temperature. Since the agreement with the H^E data is excellent, as seen in Figure 18, one may suspect uncertainty in the experimental Cp data.

Agreement with the various data sources.

In Table 13 are given the AARD values, and as seen, the agreement between the model and experimental data is generally very good. The vapor phase compositions are very well represented and much better than for MDEA and even better than for DMMEA. The volatility of MMEA is significantly lower than that of DMMEA, so this is not the reason. However, MMEA has a lower molecular weight and behaves better in the ebulliometer with more regular boiling. This makes condensate sampling easier and more representative.

Table 13. AARD for the various data sources

Data type	Source	Variable	AARD
$PTxy$	This work	P_T	0.5%
$PTxy$	This work	P_{MMEA}	7.3%
PTx	Touhara et al. (1982) [36]	P_T	4.6%
H^E	Mundhwa and Henni (2007) [63]	H^E	4.4%
H^E	Touhara et al. (1982) [36]	H^E	2.1%
Cp	Mundhwa (2007) [70]	Cp	7.0%

3.2.4. AEP-H_2O

The only binary VLE data for the AEP-water system found in the literature are partial pressure data from Du and Rochelle (2014) [11] based on FTIR for direct analysis of the gas phase.

Table 14. Available data for the AEP-H_2O system.

Source	Data type	Data points
This work, set 1	VLE (Ebulliometer), $PTxy$	75
This work, set 2	VLE (Ebulliometer), $PTxy$	10
Du and Rochelle (2014) [11]	VLE (Static cell), $P_{AEP}Tx$	10
Liang et al. [75]	Specific heat, Cp	55

All data from this work, sets 1 and 2, and data from Du and Rochelle (2014) were used in the regression. The Cp data from Liang et al. [75] were not used. The experimental data from

this work cover an AEP range of 0.01 to 0.42 in mole fraction, equivalent to 0.07 to 84 mass%. Because of uncertainties in the condensate sampling in set 2, it was decided not to use these vapor data in the model fitting but only use the results as PTx data. However, all data are given in Table B4 in the appendix. It can be noted that AEP, a triamine, only has two active amine groups and titrates down to pH 2.5 as a diamine, (see El-Sharif, et al., (2016) [74])

Two models were developed for AEP, one directly from the regressions as described above, model A, and one with parameters from model A manually tuned to fit AEP pressure data better, called model B. The regressed parameters for the NRTL models are given in Table 8, and AARDs for the various data sets are shown in Table 15.

Comparison with data

In Figure S13a) in supplementary information, the comparison between experimental total pressure data from this work and the developed models A and B is shown. We see that the regressed model A can represent the total pressure (P_T) data satisfactorily, as also shown by the AARD of 1.8%. Model B slightly over-predicts the total pressures from data set 1, but the difference from model A is less than 5%. This is more than the analytical uncertainty but taking the problem of obtaining representative samples into account, it may be within the total experimental uncertainty. For data set 2, the models are similar. The AARD for total pressure using model B, was 4%.

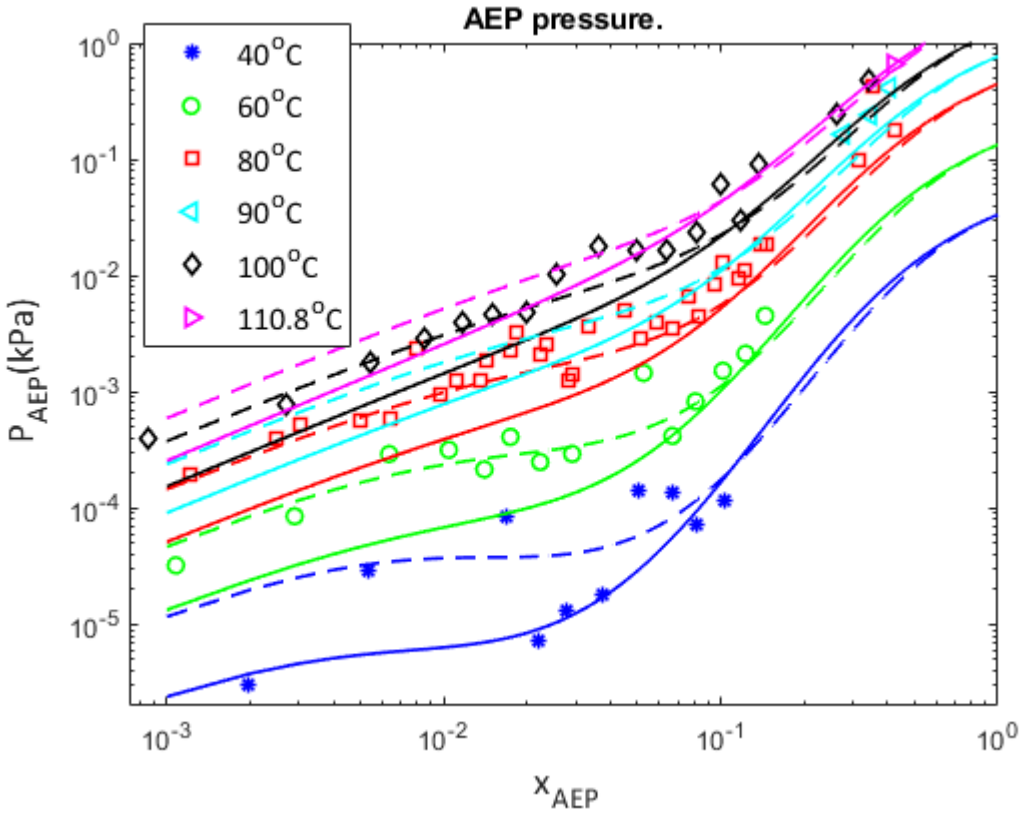

Figure 17. Experimental and predicted AEP vapor pressures from both model A and B given in Table 8. Solid lines: model A, dashed lines: model B. Blue: 40ºC, green: 60ºC, red: 80ºC, cyan: 90ºC, black: 100ºC and mauve: 110.8ºC.

Figure 17 shows experimental and predicted AEP partial pressures. Above a mole fraction of 0.1, the two model, A and B, are very similar and under-predict the vapor pressures slightly. Below 0.1 in mole fraction, model B is significantly better and follows the trends in AEP pressure. The curve for model B at 40ºC in Figure 17 is nearly flat at x_{AEP} between 0.001 and 0.003 in mole fraction. This could indicate a possible azeotrope, but more accurate data are needed to establish this

In Figure S14 and S15 in the supplementary information, modelled and experimental activity coefficients for both AEP and water are shown for model A and B respectively. With model A, the water activities are seen to be slightly over-predicted, in particular at low concentrations. For AEP, the scatter in the experimental data is large, but the model seems to give a reasonable

description down to a mole fraction of about 0.1. However, below this range, the model is incapable of replicating the relatively sharp rise in activity, which, despite the scatter, seems to be experimentally significant. Using model B, a sharp increase in AEP activity coefficient at low concentrations is realized, resulting in a better fit to the AEP pressure data as seen in Figure 17. The water activity coefficients seem over-predicted at low AEP concentrations. According to the Gibbs-Duhem relationship one would expect a bulge in the water activity coefficient in the concentration range x_{AEP} = 0-0.1 because of the increase in AEP activity coefficients at low concentrations, as predicted by the model. This is not seen in the experimental data and may point to an inconsistency between the experimental vapor phase and total pressure data in data set 1.

Figure 18 shows a comparison between model A and B and the data from Du and Rochelle (2014) [11]. These data are based on experiments in a static cell where the gas phase composition is directly measured in situ using FTIR. The FTIR detection limit is given as about 1 ppmv, equivalent to 0.1Pa. We see that the results at a mole fraction of 0.083 are predicted well for model A. This is in the range where the modelled activity coefficients are close to the experimental values, see Figure S14 in supplementary information. At the lowest concentration, with a mole fraction of 0.012, model A under-predicts the vapor phase AEP concentration by a factor of about 4. The experimental gas phase concentration levels are in the same range as for the high mole fraction, indicating that the analytical accuracy should be about the same. Model B represents the data at the lowest mole fraction, 0.012, well, but the predictions for the high mole fraction, 0.083, exceeds model A by about 20%. In order to improve the model further, more vapor pressure data are needed for low AEP concentrations.

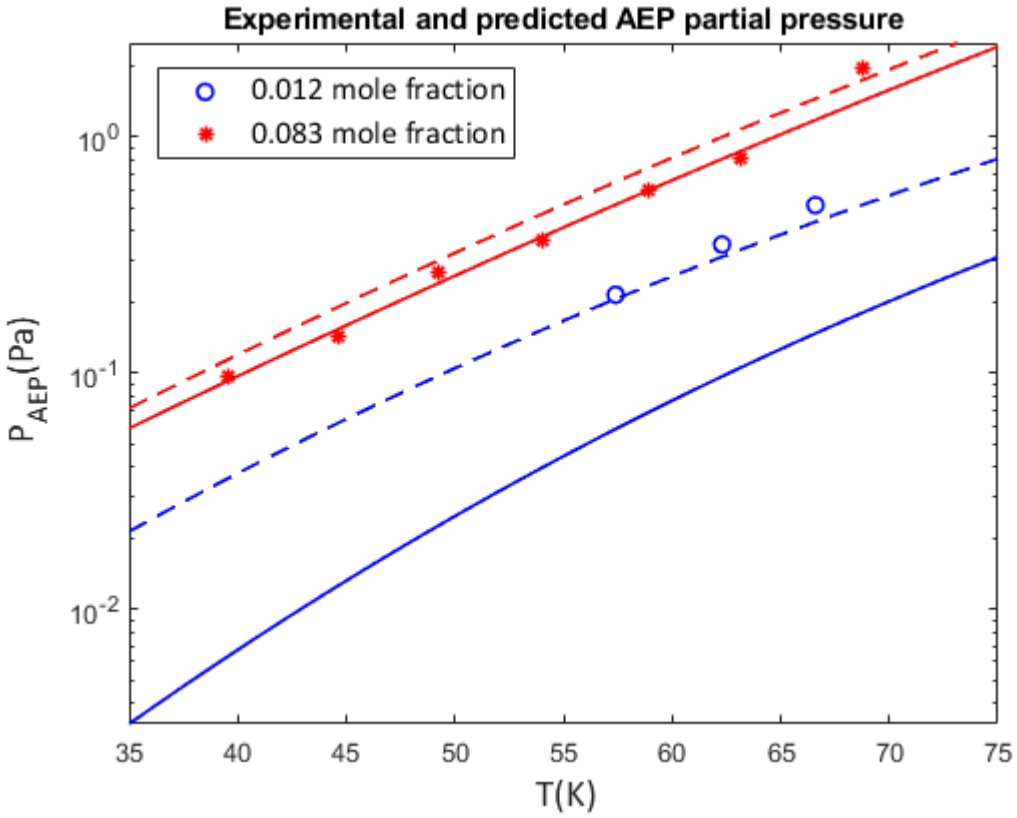

Figure 18. Predicted AEP vapor pressures compared with data from Du and Rochelle (2014) [11]. Solid lines: model A, dashed lines: model B.

Specific heat.

In supplementary information, Figure S16, a comparison between experimental and model values of specific heat is given. The experimental data are taken from Liang et al. [75] for both pure AEP and aqueous blends. Neither model A nor model B predicts the specific heats well, but model B seems to give more reasonable trends with temperature. The effect of temperature seems to be over-predicted for the lower AEP mole fractions.

Agreement with the various data sources.

In table 15 are given the AARD values for both the original NRTL model, and for model B. The original model does a better job of representing the total pressure data. However, model B

is better for all other quantities, and in particular for the AEP partial pressure predictions, as already discussed. As mentioned, model B is also somewhat better than the original model in predicting specific heat.

Table 15. AARD for the various data sources

Data type	Source	Variable	AARD**	AARD***
$PTxy$	This work	P_T	1.8%	4.0%
$PTxy$	This work	P_{AEP}	51%*	32%*
$PTxy$	Du and Rochelle (2014) [11]	P_{AEP}	28%	19%
Cp^E	Liang et al. (2016) [75]	Cp^E	12%	9%

* Because of high uncertainty, the measurements at 40°C are not included. ** Model A, ***model B

4. Conclusions

This work presents new vapor-liquid data for the pure components dimethylmonoethanolamine (DMMEA) and methylmonoethanolamine (MMEA), and for the binary systems of aqueous MDEA, DMMEA, MMEA, and AEP. New Antoine models are developed for the pure component systems, and new and improved NRTL models for the binary systems. New data from this work, all available data on VLE, excess heat of mixing, H^E, freezing point depression and specific heat data were gathered, thoroughly analyzed, and used selectively in the parameter optimization during modelling. Emphasis was put on a best possible representation of amine volatility to enable reasonable predictions of amine emissions from absorption plants and to form a basis for subsequent models of ternary systems with CO_2. Model predictions are compared with experimental results and models, source by source, and the overall results are satisfactory.

Acknowledgments

The authors acknowledge financial support from the “A Green Sea”, project performed under the Research Council of Norway Petromaks programme with partners Equinor (Statoil), Gassco and Petrobras(200455/S60) and the LAUNCH project funded through the ACT programme (Accelerating CCS Technologies, Horizon2020 Project No 299662). Financial contributions have been made by Ministry of Economic Affairs and Climate Policy, the Netherlands; The Federal Ministry for Economic Affairs and Energy, Germany; Gassnova of Norway through the CLIMIT program; and the Department for Business, Energy & Industrial Strategy, UK, with extra funding from the US Department of Energy.

Appendix A

Table A1: Pure component saturation pressures from this work*

DMMEA			MMEA		
$T/$°C	P_i^{sat}/kPa Measured	P_i^{sat}/kPa Corrected	$T/$°C	P_i^{sat}/kPa Measured	P_i^{sat}/kPa Corrected
50.64	3.79	3.77	83.099	5.17	4.94
55.28	4.79	4.77	88.469	6.75	6.46
64.01	7.29	7.25	96.446	9.9	9.49
70.45	9.79	9.74	105.592	15.0	14.41
75.61	12.29	12.22	122.844	30.6	29.50
79.74	14.79	14.71	143.681	65.47	63.28
86.69	19.79	19.68	149.858	80.54	77.90
97.11	29.79	29.61	156.61	100.1	96.88
104.99	39.78	39.53	157.134	101.8	98.53
111.34	49.79	49.47			
116.76	59.8	59.41			
121.47	69.8	69.33			
125.69	79.81	79.26			
129.42	89.78	89.16			
132.92	99.76	99.06			

*Standard uncertainty u(T) = 0.05K and u(P) = 0.15 kPa

Appendix B

Table B-1: Experimental (this work) ebulliometer data from this work for MDEA-H_2O at 313 K, 333 K, 353 K and 373 K.

$T/°K$	P/kPa	x_{MDEA}	$u(x)$	y_{MDEA}
313.008	7.07	0.0050	0.0002	0.000004
313.031	6.79	0.0121	0.0004	0.000004
313.044	6.76	0.0332	0.001	0.000002
312.985	6.68	0.0692	0.002	0.000009
313.001	6.48	0.1300	0.004	0.000020
313.053	4.87	0.2072	0.006	0.000092
313.008	4.19	0.3127	0.009	0.000360
333.027	19.58	0.0050	0.0002	0.000011
332.991	19.60	0.0122	0.0004	0.000005
333.041	19.09	0.0337	0.001	0.000004
333.039	18.49	0.0703	0.002	0.000013
333.042	17.38	0.1293	0.004	0.000032
333.004	15.38	0.2324	0.007	0.000229
333.001	11.67	0.3978	0.012	0.000413
333.003	6.31	0.7322	0.022	0.003317
353.014	47.09	0.0053	0.0002	0.000020
352.998	46.88	0.0125	0.0004	0.000013
353.024	46.08	0.0342	0.001	0.000025
353.007	44.48	0.0709	0.002	0.000059
353.002	41.79	0.1363	0.004	0.000114
353.001	36.79	0.2473	0.007	0.000348
353.036	28.99	0.4735	0.015	0.001333
353.032	11.09	0.8227	0.025	0.004211
373.008	100.88	0.0055	0.0002	0.000054
373.007	100.38	0.0125	0.0004	0.000200
373.002	98.47	0.0333	0.001	0.000068
373.012	95.47	0.0687	0.002	0.000099
373.003	90.17	0.1272	0.004	0.000307
373.003	79.87	0.2479	0.007	0.000633
373.003	58.49	0.4586	0.015	0.001939
373.002	32.27	0.7683	0.023	0.005706

*Standard uncertainty u(T) = 0.05K and u(P) = 0.15 kPa, $u_r(x)$ =3%; $u_r(y)$ =5%

Table B-2: Experimental (this work) ebulliometer data for DMMEA-H_2O at 333 K, 353 K and 373 K.*

$T/°K$	P/kPa	x_{DMMEA}	y_{DMMEA}
373.173	101.25	0.021	0.0146
373.146	101.05	0.044	0.0304
373.142	100.65	0.069	0.0448
373.136	100.13	0.095	0.0561
373.160	99.40	0.124	0.0681
373.162	98.28	0.171	0.0841
373.140	97.00	0.222	0.1027
353.179	47.15	0.020	0.0086
353.144	46.87	0.043	0.0231
353.154	46.58	0.067	0.0358
353.130	46.31	0.093	0.0440
353.158	45.80	0.123	0.0588
353.164	44.69	0.168	0.0770
353.182	43.52	0.217	0.0930
333.126	19.69	0.027	0.0076
333.117	19.49	0.050	0.0187
333.144	19.28	0.075	0.0273
333.207	19.08	0.101	0.0370
333.204	18.77	0.130	0.0474
333.233	18.28	0.177	0.0645
333.169	17.70	0.219	0.0836

*Standard uncertainty u(T) = 0.05K and u(P) = 0.15 kPa, $u_r(x) = 3\%$; $u_r(y) = 5\%$

Table B-3: Experimental (this work) ebulliometer data for MMEA-H_2O at 313K, 333 K, 353 K and 373 K.*

$T/°K$	P/kPa	x_{MMEA}	y_{MMEA}
313.20	7.28	0.0121	0.0003
313.20	7.18	0.0264	0.0007
313.20	7.08	0.0413	0.0012
313.24	6.96	0.0589	0.0017
313.19	6.67	0.0964	0.0030
313.13	6.28	0.1421	0.0047
333.18	19.67	0.0117	0.0005
333.13	19.37	0.0262	0.0011
333.13	19.08	0.0431	0.0022
333.11	18.78	0.0588	0.0029
333.16	18.17	0.0963	0.0043
333.13	17.27	0.1442	0.0071
333.14	16.17	0.2045	0.0102
353.13	46.69	0.0113	0.0009
353.12	46.18	0.0226	0.0018
353.16	45.68	0.0385	0.0028
353.13	44.98	0.0553	0.0039
353.12	43.58	0.0914	0.0065
353.16	41.78	0.1415	0.0104
353.15	39.28	0.2029	0.0157
373.14	99.91	0.0117	0.0014
373.15	98.58	0.0282	0.0032
373.16	97.51	0.0436	0.0048
373.15	96.21	0.0601	0.0064
373.16	90.04	0.1423	0.0150
373.14	85.34	0.2028	0.0213
373.14	79.08	0.2772	0.0311

*Standard uncertainty u(T) = 0.05K and u(P) = 0.15 kPa, $u_r(x) = 3\%$; $u_r(y) = 5\%$

Table B-4: Experimental (this work) ebulliometer data for AEP-H_2O at 313K, 333 K, 353 K and 373 K.

$T/°K$	P/kPa	x_{AEP}	y_{AEP}
313.06	7.38	0.0007	1.08E-08**
313.11	7.38	0.0020	4.14E-07
313.17	7.38	0.0053	3.86E-06*
312.99	7.28	0.0090	1.80E-07
313.08	7.28	0.0125	2.16E-07
313.17	7.27	0.0168	1.16E-05*
313.07	7.18	0.0220	1.01E-06
313.22	7.18	0.0275	1.82E-06
313.22	7.07	0.0372	2.59E-06
313.20	6.87	0.0504	2.02E-05*
313.13	6.57	0.0669	2.04E-05*
313.15	6.28	0.0819	1.13E-05
313.08	5.88	0.1034	1.95E-05
333.13	19.97	0.0011	1.62E-06
333.16	19.97	0.0029	4.29E-06
333.14	19.87	0.0063	1.48E-05
333.13	19.78	0.0104	1.61E-05
333.13	19.69	0.0140	1.10E-05
333.10	19.58	0.0174	2.10E-05
333.12	19.48	0.0223	1.29E-05
333.17	19.31	0.0291	1.52E-05
333.20	18.57	0.0526	7.86E-05*
333.18	17.98	0.0669	2.34E-05
333.17	17.28	0.0810	4.81E-05
333.12	16.28	0.1017	9.36E-05
333.20	15.27	0.1229	1.40E-04
333.11	13.87	0.1445	3.27E-04
353.17	47.58	0.0030	1.12E-05
353.16	47.38	0.0064	1.24E-05
353.16	47.22	0.0097	2.02E-05
353.16	47.01	0.0135	2.64E-05
353.20	46.68	0.0175	4.98E-05
353.12	46.39	0.0223	4.50E-05
353.20	46.19	0.0281	2.78E-05
353.17	45.49	0.0292	3.18E-05
353.19	44.49	0.0513	6.54E-05
353.21	43.28	0.0665	8.06E-05
353.16	41.68	0.0827	1.06E-04
353.18	39.69	0.1019	3.23E-04
353.21	37.48	0.1224	2.96E-04
353.16	35.29	0.1388	5.20E-04
353.17	47.58	0.0012	4.12E-06

353.15	47.48	0.0025	8.50E-06
353.15	47.38	0.0050	1.18E-05
353.17	47.28	0.0080	5.02E-05
353.16	47.08	0.0111	2.73E-05
353.14	46.88	0.0143	3.99E-05
353.15	46.68	0.0182	6.98E-05
353.14	46.38	0.0234	5.58E-05
353.15	45.78	0.0335	8.00E-05
353.15	44.98	0.0447	1.12E-04
353.18	43.88	0.0590	9.17E-05
353.18	42.28	0.0764	1.57E-04
353.18	40.39	0.0954	2.07E-04
353.14	38.09	0.1167	2.53E-04
353.16	34.89	0.1465	5.46E-04
373.14	101.78	0.0009	3.91E-06
373.16	101.67	0.0027	7.85E-06
373.17	101.37	0.0054	1.80E-05
373.16	100.98	0.0084	2.93E-05
373.14	100.58	0.0117	3.95E-05
373.16	100.28	0.0151	4.68E-05
373.16	99.78	0.0198	4.78E-05
373.15	99.08	0.0254	1.05E-04
373.14	97.58	0.0364	1.85E-04
373.16	95.68	0.0500	1.74E-04
373.15	93.38	0.0641	1.76E-04
373.17	90.48	0.0811	2.62E-04
373.13	86.98	0.1003	6.95E-04*
373.14	83.37	0.1183	3.59E-04
373.20	78.98	0.1367	1.15E-03
353.25	15.77	0.4272	1.13E-2
353.55	20.77	0.3133	4.74E-3
354.75	20.77	0.3531	2.07E-2*
362.95	34.77	0.2767	4.71E-3
363.35	30.28	0.3464	7.90E-3
363.85	26.77	0.4060	1.54E-2
373.25	54.77	0.2611	4.45E-3
373.45	41.77	0.4095	3.08E-2*
373.95	48.77	0.3410	9.68E-3
383.95	57.77	0.4190	1.13E-2

*Vapor composition considered outlier. **At detection limit

Standard uncertainty u(T) = 0.05K and u(P) = 0.15 kPa, $u_r(x)$ =3%; $u_r(y)$ =5%

References

[1] A. Hartono, R. Ahmad, H.F. Svendsen, H.K. Knuutila, New solubility and heat of absorption data for CO2 in blends of 2-amino-2-methyl-1-propanol (AMP) and Piperazine (PZ) and a new eNRTL model representation, Fluid Phase Equilibria, 550 (2021) 113235, https://doi.org/10.1016/j.fluid.2021.113235.

[2] D.D.D. Pinto, H. Knuutila, G. Fytianos, G. Haugen, T. Mejdell, H.F. Svendsen, CO_2 post combustion capture with a phase change solvent. Pilot plant campaign, International Journal of Greenhouse Gas Control, 31 (2014) 153-164,http://dx.doi.org/10.1016/j.ijggc.2014.10.007.

[3] D.D.D. Pinto, S.A.H. Zaidy, A. Hartono, H.F. Svendsen, Evaluation of a phase change solvent for CO2 capture: Absorption and desorption tests, International Journal of Greenhouse Gas Control, 28 (2014) 318-327,https://doi.org/10.1016/j.ijggc.2014.07.002.

[4] Max Appl, Ulrich Wagner, Hans J. Henrici, Klaus Kuessner, Klaus Volkamer, Ernst Fuerst, Removal of CO2 and/or H2 S and/or COS from gases containing these constituents, B. SE (Ed.), 1980.

[5] I. Eide-Haugmo, O.G. Brakstad, K.A. Hoff, K.R. Sørheim, E.F. da Silva, H.F. Svendsen, Environmental impact of amines, Energy Procedia, 1 (2009) 1297-1304,https://doi.org/10.1016/j.egypro.2009.01.170.

[6] I. Eide-Haugmo, O.G. Brakstad, K.A. Hoff, E.F. da Silva, H.F. Svendsen, Marine biodegradability and ecotoxicity of solvents for CO2-capture of natural gas, International Journal of Greenhouse Gas Control, 9 (2012) 184,https://doi.org/10.1016/j.ijggc.2012.03.006.

[7] A. Henni, J. Li, P. Tontiwachwuthikul, Reaction Kinetics of CO2 in Aqueous 1-Amino-2-Propanol, 3-Amino-1-Propanol, and Dimethylmonoethanolamine Solutions in the Temperature Range of 298−313 K Using the Stopped-Flow Technique, Industrial & Engineering Chemistry Research, 47 (2008) 2213-2220,https://doi.org/10.1021/ie070587r.

[8] A. Hedayati, F. Feyzi, CO2-binding organic liquids for high pressure CO2 absorption: Statistical mixture design approach and thermodynamic modeling of CO2 solubility using LJ-Global TPT2 EoS, Journal of Molecular Liquids, 337 (2021) 116396,https://doi.org/10.1016/j.molliq.2021.116396.

[9] G. Rochelle, E. Chen, S. Freeman, D. Van Wagener, Q. Xu, A. Voice, Aqueous piperazine as the new standard for CO2 capture technology, Chemical Engineering Journal, 171 (2011) 725-733,https://doi.org/10.1016/j.cej.2011.02.011.

[10] Bartholome Ernst, Schmidt Hans Wilhelm, F. Juergen, Process for removing carbon dioxide from gas mixtures, 1971.

[11] Y. Du, G.T. Rochelle, Thermodynamic Modeling of Aqueous Piperazine/N-(2-Aminoethyl) Piperazine for CO2 Capture, Energy Procedia, 63 (2014) 997-1017,https://doi.org/10.1016/j.egypro.2014.11.108.

[12] A. Dey, S.K. Dash, S.C. Balchandani, B. Mandal, Investigation on the inclusion of 1-(2-aminoethyl) piperazine as a promoter on the equilibrium CO2 solubility of aqueous 2-amino-2-methyl-1-propanol, Journal of Molecular Liquids, 289 (2019) 111036,https://doi.org/10.1016/j.molliq.2019.111036.

[13] S.A. Freeman, R. Dugas, D.H. Van Wagener, T. Nguyen, G.T. Rochelle, Carbon dioxide capture with concentrated, aqueous piperazine, International Journal of Greenhouse Gas Control, 4 (2010) 119-124,http://dx.doi.org/10.1016/j.ijggc.2009.10.008.

[14] S.A. Mazari, B.S. Ali, B.M. Jan, I.M. Saeed, Degradation study of piperazine, its blends and structural analogs for CO2 capture: A review, International Journal of Greenhouse Gas Control, 31 (2014) 214-228,http://dx.doi.org/10.1016/j.ijggc.2014.10.003.

[15] M. Rogalski, S. Malanowski, Ebulliometers modified for the accurate determination of vapour—liquid equilibrium, Fluid Phase Equilibria, 5 (1980) 97-112,http://dx.doi.org/10.1016/0378-3812(80)80046-X.

[16] I. Kim, H.F. Svendsen, E. Børresen, Ebulliometric Determination of Vapor-Liquid Equilibria for Pure Water, Monoethanolamine, N-Methyldiethanolamine, 3-(Methylamino)-propylamine, and Their Binary and Ternary Solutions, Journal of Chemical & Engineering Data, 53 (2008) 2521-2531,https://doi.org/10.1021/je800290k.
[17] A. Hartono, F. Saleem, M.W. Arshad, M. Usman, H.F. Svendsen, Binary and ternary VLE of the 2-(diethylamino)-ethanol (DEEA)/3-(methylamino)-propylamine (MAPA)/water system, Chemical Engineering Science, 101 (2013) 401-411,http://dx.doi.org/10.1016/j.ces.2013.06.052.
[18] A. Hartono, M. Saeed, A.F. Ciftja, H.F. Svendsen, Binary and ternary VLE of the 2-amino-2-methyl-1-propanol (AMP)/piperazine (Pz)/water system, Chemical Engineering Science, 91 (2013) 151-161,https://doi.org/10.1016/j.ces.2013.01.015.
[19] A.A. Trollebø, A. Hartono, M. Usman, M. Saeed, H.F. Svendsen, Vapour-liquid equilibria in pure N-Methyl-1,3-diaminopropane (MAPA), 1,3-diaminopropane (DAP), 2-(Isopropylamino)ethanol (IPAE), N-tert-Butyldiethanolamine (N-TBDEA) and their aqueous solutions, The Journal of Chemical Thermodynamics, 141 (2020),https://doi.org/10.1016/j.jct.2019.105965.
[20] A. Hartono, C. Nøkleby, I. Kim, H.K. Knuutila, Vapor–Liquid Equilibria Data for 2-Piperidineethanol and 1-(2-Hydroxyethyl)pyrrolidine in Aqueous Solutions and a UNIQUAC Model Representation, Journal of Chemical & Engineering Data, 67 (2022) 159-166,https://doi.org/10.1021/acs.jced.1c00726.
[21] C. Antoine, Tensions des vapeurs; nouvelle rrelation eentre les tensions et les températures, Comptes Rendus des Séances de l'Académie des Sciences, 107 (681-684), 107 (1888) 778-780, 836-837.
[22] H. Renon, J.M. Prausnitz, Local compositions in thermodynamic excess functions for liquid mixtures, AIChE Journal, 14 (1968) 135-144,https://doi.org/10.1002/aic.690140124.
[23] J.M. Prausnitz, R.N. Lichtenthaler, E. Gomes de Azevedo, Molecular Thermodynamics of Fluid-Phase Equilibria, Prentice Hall PTR, Upper Saddle River, N.J, 1999.
[24] K.A.G. Schmidt, Y. Maham, A.E. Mather, Use of the NRTL equation for simultaneous correlation of vapour-liquid equilibria and excess enthalpy, Journal of Thermal Analysis and Calorimetry, 89 (2007) 61-72,https://doi.org/10.1007/s10973-006-8307-6.
[25] D.-Y. Peng, D.B. Robinson, A New Two-Constant Equation of State, Industrial & Engineering Chemistry Fundamentals, 15 (1976) 59-64,https://doi.org/10.1021/i160057a011.
[26] J. Kennedy, R. Eberhart, Particle swarm optimization, Proceedings of ICNN'95 - International Conference on Neural Networks, 4 (1995) 1942-1948 vol.1944,https://doi.org/10.1109/ICNN.1995.488968.
[27] J.G.M.S. Monteiro, D.D.D. Pinto, S.A.H. Zaidy, A. Hartono, H.F. Svendsen, VLE data and modelling of aqueous N,N-diethylethanolamine (DEEA) solutions, International Journal of Greenhouse Gas Control, 19 (2013) 432-440,https://doi.org/10.1016/j.ijggc.2013.10.001.
[28] K. L., M. H., Ueber das aethanolmethylamin und Diäthanolmethylamin, , Berichte der Deutschen chemischen Gesellschaft, 31 (1898) 1069-1072.
[29] O. Noll, A. Valtz, D. Richon, T. Getachew-Sawaya, I. Mokbel, J. Jose, Vapor pressures and liquid densities of N-methylethanolamine, diethanolamine, and N-methyldiethanolamine, ELDATA: Int. Electron. J. Phys.-Chem. Data, 4 (1998) 105-120.
[30] A. Soames, A. Al Helal, S. Iglauer, A. Barifcani, R. Gubner, Experimental Vapor–Liquid Equilibrium Data for Binary Mixtures of Methyldiethanolamine in Water and Ethylene Glycol under Vacuum, Journal of Chemical & Engineering Data, 63 (2018) 1752-1760,https://doi.org/10.1021/acs.jced.8b00054.
[31] D.M. VonNiederhausern, G.M. Wilson, N.F. Giles, Critical Point and Vapor Pressure Measurements for Four Compounds by a Low Residence Time Flow Method, Journal of Chemical & Engineering Data, 51 (2006) 1986-1989,https://doi.org/10.1021/je0602465.

[32] C. Dell'Era, P. Uusi-Kyyny, E.-L. Rautama, M. Pakkanen, V. Alopaeus, Thermodynamics of aqueous solutions of methyldiethanolamine and diisopropanolamine, Fluid Phase Equilibria, 299 (2010) 51-59,https://doi.org/10.1016/j.fluid.2010.08.026.
[33] T. Daubert, G. Hutchison, Vapor pressure of 18 pure industrial chemicals, AIChE Symp. Ser, 1990, pp. 93-114.
[34] D. T.E., Experimental Results Phase Equilibrium Pure Compn. Prop., J.D.K.e.A.I.C.E.N.Y. Cunningham J.R., USA (Ed.) DIPPR Data ser., 1994, pp. 143.
[35] D.M. VonNiederhausern, G.M. Wilson, N.F. Giles, Critical Point and Vapor Pressure Measurements for 17 Compounds by a Low Residence Time Flow Method, Journal of Chemical & Engineering Data, 51 (2006) 1990-1995,https://doi.org/10.1021/je0602465.
[36] H. Touhara, S. Okazaki, F. Okino, H. Tanaka, K. Ikari, K. Nakanishi, Thermodynamic properties of aqueous mixtures of hydrophilic compounds 2. Aminoethanol and its methyl derivatives, The Journal of Chemical Thermodynamics, 14 (1982) 145-156,https://doi.org/10.1016/0021-9614(82)90026-X.
[37] E. Skylogianni, C. Perinu, B.Y. Cervantes Gameros, H.K. Knuutila, Carbon dioxide solubility in mixtures of methyldiethanolamine with monoethylene glycol, monoethylene glycol–water, water and triethylene glycol, The Journal of Chemical Thermodynamics, 151 (2020) 106176,https://doi.org/10.1016/j.jct.2020.106176.
[38] Y. Zhang, C.-C. Chen, Thermodynamic Modeling for CO2 Absorption in Aqueous MDEA Solution with Electrolyte NRTL Model, Industrial & Engineering Chemistry Research, 50 (2011) 163-175,https://doi.org/10.1021/ie1006855.
[39] J. Na, B.-M. Min, J.-H. Moon, J.-S. Lee, H.Y. Shin, Isothermal Vapor–Liquid Equilibrium Data for Water + Diisopropanolamine, Water + N-Methyldiethanolamine and Diisopropanolamine + N-Methyldiethanolamine Systems, Int J Thermophys, 39 (2018) 96,https://doi.org/10.1007/s10765-018-2415-y.
[40] K. Klepáčová, P.J.G. Huttenhuis, P.W.J. Derks, G.F. Versteeg, Vapor Pressures of Several Commercially Used Alkanolamines, Journal of Chemical & Engineering Data, 56 (2011) 2242-2248,https://doi.org/10.1021/je101259r.
[41] N. Chiali-Baba-Ahmed, F. Dergal, L. Negadi, I. Mokbel, Measurement and correlation of the (vapor+liquid) equilibria of pure 4-ethylmorpholine, 1,2-dimethylisopropylamine and N,N-dimethylethanolamine, and their binary aqueous solutions, The Journal of Chemical Thermodynamics, 63 (2013) 44-51,https://doi.org/10.1016/j.jct.2013.03.020.
[42] K. Quitzsch, H.-P. Hofmann, D. Hering, R. Salzer, G. Geiseler, Über isobare flüssigkeit dampf-gleichgewichte binärer und ternärer mischungen aus ethyglykol, dimethylaminoäthanol und 2-(2.dimethylaminoäthoxy-)äthanol, Z. Phys. Chem. (Leipzig), 243 (1970) 321-339.
[43] S. Kapteina, K. Slowik, S.P. Verevkin, A. Heintz, Vapor Pressures and Vaporization Enthalpies of a Series of Ethanolamines, Journal of Chemical & Engineering Data, 50 (2005) 398-402,https://doi.org/10.1021/je049761y.
[44] A. Hartono, A. Rafiq, S. Gondal, H.F. Svendsen, Solubility data for Nitrous Oxide (N2O) and Carbon dioxide (CO2) in Piperazine (PZ) and a new eNRTL model, Fluid Phase Equilibria, 538 (2021) 112992,https://doi.org/10.1016/j.fluid.2021.112992.
[45] G. Bringas, P. Navarro-Santos, R. López-Rendón, J. López-Lemus, F. Bresme, Molecular Dynamics Simulations of 2-(Dimethylamino)ethanol (DMEA), The Journal of Physical Chemistry B, 119 (2015) 5035-5046,https://doi.org/10.1021/jp509577x.
[46] R.M.M. Stephenson, Stanislaw Handbook of the thermodynamics of organic compounds. , 1989.
[47] DIPPR-801, The Information and Data Evaluation Manager for Design Institute for Physical Properties, Version 4.1.0., 2004.
[48] W.V. Steele, R.D. Chirico, S.E. Knipmeyer, A. Nguyen, Vapor Pressure, Heat Capacity, and Density along the Saturation Line, Measurements for Cyclohexanol, 2-Cyclohexen-1-one, 1,2-

Dichloropropane, 1,4-Di-tert-butylbenzene, (±)-2-Ethylhexanoic Acid, 2-(Methylamino)ethanol, Perfluoro-n-heptane, and Sulfolane, Journal of Chemical & Engineering Data, 42 (1997) 1021-1036,https://doi.org/10.1021/je9701036.
[49] S. H., P. H., R. H., Synthese des Kreatinols (N-Methyl-N-(β-oxäthyl)-guanidin). 2. Mitteilungen über studien in der Guanidinreihe. , Hoppe-Zeyler's Z. Physiol. Chem 174 (1928) 119-176.
[50] Huntsman, AEP-HP 2022.
[51] Sigma-Aldrich, 1-(2-Aminoethyl)piperazine CAS 140-31-8, 2022.
[52] C. Databook, N-Aminoethylpiperazine CAS#: 140-31-8, 2022.
[53] A.A. Efimova, V.N. Emel'yanenko, S.P. Verevkin, Y. Chernyak, Vapour pressure and enthalpy of vaporization of aliphatic poly-amines, The Journal of Chemical Thermodynamics, 42 (2010) 330-336,https://doi.org/10.1016/j.jct.2009.09.003.
[54] Parchem, N-Aminoethylpiperazine-007530.pdf, 2022.
[55] C.L. Yaws, P.K. Narasimhan, C. Gabbula, Yaws' Handbook of Antoine Coefficients for Vapor Pressure (2nd Electronic Edition), Gulf Professional Publishing, 2015.
[56] S. Xu, S. Qing, Z. Zhen, C. Zhang, J.J. Carroll, Vapor pressure measurements of aqueous N-methyldiethanolamine solutions, Fluid Phase Equilibria, 67 (1991) 197-201,https://doi.org/10.1016/0378-3812(91)90055-C.
[57] B.-T.N. Nguyen, Amine Volatility in CO2 Capture. , Department of Chemical Engineering Ph.D Thesis, The University of Texas at Austin, Austin, 2013.
[58] B.S. Kuwairi, Vapor Pressure of Selected Pure Materials and Mixtures, Oklahoma State, University, 1983.
[59] R. Sidi-Boumedine, S. Horstmann, K. Fischer, E. Provost, W. Fürst, J. Gmehling, Experimental determination of carbon dioxide solubility data in aqueous alkanolamine solutions, Fluid Phase Equilibria, 218 (2004) 85-94,https://doi.org/10.1016/j.fluid.2003.11.014.
[60] Y. Maham, L. G. Hepler, A. E. Mather, A. W. Hakin, R. A. Marriott, Molar heat capacities of alkanolamines from 299.1 to 397.8 K Group additivity and molecular connectivity analyses, Journal of the Chemical Society, Faraday Transactions, 93 (1997) 1747-1750,http://dx.doi.org/10.1039/A607568A.
[61] M.L. Posey, Thermodynamic Model for Acid Gas Loaded Alkanolamine Solution., Chemical Engineering, University o fTexas at Austin,TX, USA, Texas, 1996.
[62] Y. Maham, A.E. Mather, C. Mathonat, Excess properties of (alkyldiethanolamine +H2O) mixtures at temperatures from (298.15 to 338.15) K, The Journal of Chemical Thermodynamics, 32 (2000) 229-236,https://doi.org/10.1006/jcht.1999.0595.
[63] M. Mundhwa, A. Henni, Molar Heat Capacity of Various Aqueous Alkanolamine Solutions from 303.15 K to 353.15 K, Journal of Chemical & Engineering Data, 52 (2007) 491-498,https://doi.org/10.1021/je0604232.
[64] E. Voutsas, A. Vrachnos, K. Magoulas, Measurement and thermodynamic modeling of the phase equilibrium of aqueous N-methyldiethanolamine solutions, Fluid Phase Equilibria, 224 (2004) 193-197,https://doi.org/10.1016/j.fluid.2004.05.012.
[65] P.L. Fosbøl, M.G. Pedersen, K. Thomsen, Freezing Point Depressions of Aqueous MEA, MDEA, and MEA−MDEA Measured with a New Apparatus, Journal of Chemical & Engineering Data, 56 (2011) 995-1000,https://doi.org/10.1021/je100994v.
[66] H.T. Chang, M. Posey, G.T. Rochelle, Thermodynamics of Alkanolamine Water Solutions from Freezing-Point Measurements, Industrial & Engineering Chemistry Research, 32 (1993) 2324-2335,https://doi.org/10.1021/ie00022a016.
[67] J. Wisniak, The Herington test for thermodynamic consistency, Industrial & Engineering Chemistry Research, 33 (1994) 177-180,https://doi.org/10.1021/ie00025a025.

[68] H.C. Van Ness, Thermodynamics in the treatment of vapor/liquid equilibrium (VLE) data, Pure and Applied Chemistry, 67 (1995) 859,https://doi.org/10.1351/pac199567060859.
[69] X. Ge, X. Wang, Calculations of Freezing Point Depression, Boiling Point Elevation, Vapor Pressure and Enthalpies of Vaporization of Electrolyte Solutions by a Modified Three-Characteristic Parameter Correlation Model, Journal of Solution Chemistry, 38 (2009) 1097-1117,https://doi.org/10.1007/s10953-009-9433-0.
[70] M. Mundhwa, Calorimetric measurements of the molar heat capacity and the molar excess enthalpy for various alkanolamines in aqueous solutions, University of Regina, Regina, 2007.
[71] T.A. Hayden, T.G.A. Smith, A.E. Mather, Heat capacity of aqueous methyldiethanolamine solutions, Journal of Chemical & Engineering Data, 28 (1983) 196-197,https://doi.org/10.1021/je00032a020.
[72] Y.-J. Chen, M.-H. Li, Heat Capacity of Aqueous Mixtures of Monoethanolamine with 2-Amino-2-methyl-l-propanol, Journal of Chemical & Engineering Data, 46 (2001) 102-106,https://doi.org/10.1021/je000146d.
[73] Shokouhi M., Jalili A.H., M. Hosseini-Jenab, Thermo Physical Properties of Some Physical and Chemical Solvents at Atmospheric Pressure, Iranian Journal of Chemical Engineering(IJChE), 10 (2013) 43-54,http://www.ijche.com/article_11673.html.
[74] A.A. El-Sherif, M.R. Shehata, M.M. Shoukry, N. Mahmoud, Potentiometric Study of Speciation and Thermodynamics of Complex Formation Equilibria of Diorganotin(IV) Dichloride with 1-(2-Aminoethyl)piperazine, Journal of Solution Chemistry, 45 (2016) 410-430,https://doi.org/10.1007/s10953-016-0450-5.
[75] K.-L. Liang, R.B. Leron, M.-H. Li, Heat capacities of aqueous binary and ternary mixtures (with piperazine) of N-(2-aminoethyl)-piperazine and N,N,N′-trimethylethylenediamine at temperatures (303.2–353.2)K, The Journal of Chemical Thermodynamics, 103 (2016) 51-58,https://doi.org/10.1016/j.jct.2016.08.006.